
**UNDERSTANDING DOME-BUILDING ERUPTIONS:
A RHEOLOGICAL AND ACOUSTIC STUDY**

Yan Lavallée

Dissertation
an der Fakultät für Geowissenschaften
der Ludwig-Maximilians-Universität
München

vorgelegt von
Yan Lavallée
aus St-Jérôme, Québec, Canada

München, den 21. November, 2007

Erstgutachter:

DONALD B. DINGWELL

Zweitgutachter:

JÖRN H. KRUHL

Tag der mündlichen Prüfung:

7. February, 2008

[...] and Pachamama trembled, for long it roar and longer it went on, and before exhaustion,
fire slit its throat and cinders went tumbling down the slopes of Tungurahua;

I was high up, over there, and saw everything

Later it settled...

...the next day, the riders stormed by and stirred it all again.

We can look at the photographs later [...]

- telltale of a friend who witness the August
2006 eruption of Tungurahua, Ecuador



...Maman, on est quoi?

Table of Content

i) List of figures	ix
ii) List of tables	x
iii) Acknowledgments	xi
iv) Preamble	xiii
v) Summary	xiv
vi) Zusammenfassung	xvi
Chapter 1. Introduction	21
1.1. lava rheology	22
1.2. Seismogenic volcanic conduits	25
1.3. Acoustic Emission (AE)	26
1.4. Failure Forecast Method (FFM)	27
1.5. Uniaxial compression experiments	28
Chapter 2. High-load, high-temperature deformation apparatus for synthetic and natural silicate melts)	32
2.1. Introduction	33
2.2. Instrument design	34
2.3. Parralel-plate-type viscosity measurements	35
2.4. Results on the NIST reference material SRM 717a	36
Chapter 3. A non-Newtonian rheological law for highly-crystalline dome lavas)	41
3.1. Introduction	42
3.2. Measurement method and viscosity determination	43
3.3. Results	44
3.4. Singular non-Newtonian Description of strain rate	46
3.5. General non-Newtonian rheological law	49

Chapter 4. Seismogenic lavas: fracture and eruption forecasting).....	53
4.1. Introduction.....	54
4.2. Method and calibration.....	55
4.3. Seismogenic profile across the ductile to brittle field.....	58
4.4. Application of the failure forecast method (FFM).....	61
 Chapter 5. Conclusions.....	 66
5.1. Conclusions.....	66
5.2. References.....	67
5.3. Curriculum Vitae.....	73

List of Figures

Chapter 1. Introduction

Figure 1-1. Sketch of the glass transition field.....	22
Figure 1-2. Effects of crystal fraction on the relative viscosity of a melt.....	23
Figure 1-3. Repeated fracture and healing cycles.....	26
Figure 1-4. Seismic records of an explosion at Colima volcano, august 2005.....	28

Chapter 2.

Figure 2-1. Sketch of the uniaxial press.....	34
Figure 2-2. Viscosity data obtained for different initial conditions.....	37
Figure 2-3. Obtained viscosity data compared to the certified values.....	38

Chapter 3.

Figure 3-1. Typical viscosity profile for experiments at 940 °C.....	45
Figure 3-2. Post-experiment textures.....	46
Figure 3-3. Stress-Strain-rate profile of experiments at 940 °C.....	47
Figure 3-4. Viscosity-strain-rate profiles for all experiments.....	48

Chapter 4.

Figure 4-1. Sketch of the experimental setup.....	56
Figure 4-2. Background noise calibration experiments.....	57
Figure 4-3. Experimental results for deformation of a Colima melt at 8, 16 and 24 MPa.....	59
Figure 4-4. AE absolute energy released rates for Colima and Bezymianny lavas.....	60
Figure 4-5. Anisotropy changes associated with deformation.....	61
Figure 4-6. Application of the FFM on a Colima lava.....	63

List of Tables

Chapter 2.

Table 2-1 Results for experiments on the SRM reference material 717a.....	37
---	----

Chapter3.

Table 3-1 Normalized geochemical composition of 12 measurements on glass phase of each sample.....	44
Table 3-2 Petrological and textural characteristics of rock samples.....	44
Table 3-3.....	48

Acknowledgments

My surrounding pushed me to break lavas, I broke my hand
Some of them taught me Bavarian, I thank you once again;
now I lift this glass and drink to that, Merci Bursh'!!

I am now refreshed with the idea that this work comes to an end, and it does so because of all of you around (including, all the train operators who brought me daily from Regensburg to Munich and back during my first year).

I first thank all of you who lay their eyes on these words. You are most likely a friend. I thank you for who you are and what we share!

Thanks Don Dingwell for convincing me to do a PhD on dome lavas rheology. You set the ground for an amazing study and gave me the freedom to carry it independently, yet with support and resources. You succeeded!

Kai-Uwe Hess, you were a great resource and friend! ...and patient with my ups and downs!

Yes, bureaucracy is kind of crazy everywhere- it took me three years to realize that it is the same mess whether here, in the USA, oder Heimat in Kanada. I clap my hands to Greta Barbi, Margot Lieske, Renata Döring Frank, Sandra Bauer, Yvonne Nessler, and Helen Pfuhl.

Thanks compatriot Erika Vyeveaceous for your invaluable help to make my studentship legit; nice hair!

Et Benoit Cordonnier, tu sais le faire à ta façon, et de bonne façon. *Brav ha ho trugarekaat !* Tu me fus très utile et de bonne compagnie, ici et là. Caribou Nutsy!

A Dominique ou a Pommelle- ça 'a aidé que tu sois là, j'ai po perdu mon jouale. [en passant, comment épelles-tu le nom de ton p'tit? Avec lly ou li?]

Thanks to Hugh Tuffen for paving the early way, shall I say the early day, of my study of lava rheology.

Thanks to Cristina de Campos for the laundry machine, but also for very appreciated help here, and there, and in between.

Saskia Bernstein and Jan Pawlowski were great; actually, a very great help during the microprobe analyses.

Thanks to disorder of my own, or of friends, to keep me sailing the warm grey sea.

And this most excellent guidance by most excellent Dr. dude Alfonso F. Davila Esquire.

And then you – Ulli, Basti, Bettybettybetty Beca, Wolfgang, Stephan, Christoph, Felix, Saskia, Tini and Laumi – thanks for being some of them!

Maria, Sasha, Christoph, Alfonso, Monika, Giampiero, and Marene (I guess), thanks for enduring me, my loudness, my cooking late in the night, and my lunacy; you were all great roommates

Thanks to Diana (Snüpp) Schebler for getting me over to Germany

Jonathan Castro, I am certainly grateful for this nice fieldwork in Ecuador; a bummer we didn't go back this year, but you know...

I give also many thanks to Oliver Spieler and Philip Courtial for the development of the press and many helpful recommendations throughout the laboratory work.

Abstract thoughts popped here and there and express my sweat thanks to Ines Hirsch for coping with them.

And to this, I add a last minute thanks to Kilian Scharrer for helping me with the PhD requirements, and the printing of the thesis.

Thanks also to those who nicely paid to get me through this costly endeavour. THESIS provided me with more funds and opportunity than what is often allocated to students; I am very appreciative. To my bank at home, Les Fondations Desjardins, who gave me enough dough to feed a grown up man for a year.

Ca y est j'ai faim, I'm off for a Bavarian coffee at Tresz. See you in 5 min,

- him, who thanks the exceptional extrapolation of imagination, *aka* Yan La Banane

Preamble

Part of the data presented in this doctoral dissertation have been published in scientific journals or are in the review process; namely,

Cordonnier, B., Hess, K.U., Lavallée, Y. and Dingwell, D.B., in Review. Rheology of Unzen dome lava. Submitted to *Bulletin of Volcanology*.

Hess, K.U., Cordonnier, B., Lavallée, Y. and Dingwell, D.B., 2007. High-load, high-temperature deformation apparatus for synthetic and natural silicate melts. *Review of Scientific Instruments*, 78.

Hess, K.U., Cordonnier, B., Lavallée, Y. and Dingwell, D.B., in review. Viscous heating in rhyolite: an in situ determination. Submitted to *Earth and Planetary Science Letters*.

Lavallée, Y., Hess, K.U., Cordonnier, B. and Dingwell, D.B., 2007. A non-Newtonian rheological law for highly-crystalline dome lavas. *Geology*, 35: 843-846.

Lavallée, Y., Meredith P.G., Dingwell, D.B., Hess, K.-U., Wassermann, J., Cordonnier, B., A. Gerik, J.H. Kruhl, 2008. Seismogenic lavas: fracture and eruption forecasting. Submitted in *Nature*, 453: 507-510.

Summary

Dome-building eruption models currently lack a fundamental description of the rheology and seismogenicity of lavas carrying crystals and bubbles. Especially an understanding of their transition from a ductile to a brittle behaviour is essential to forecasting the transition from effusive to explosive volcanism. A unique high-load, high-temperature uniaxial press was developed to study the rheology and seismogenicity of silicate melts and magmatic suspensions under conditions relevant to volcanic systems; but more specifically, as they are forced across the ductile to brittle transition. This new apparatus is designed to operate at constant stresses (up to 300 kN) or constant strain rates ($\sim 10^{-7}$ and 10^0 s^{-1}) and further allows us to carry on experiments on samples with high viscosities (10^8 and 10^{12} Pa s). The rheological instrument represents an advance in that it accommodates homogeneously heated samples ($\pm 2 \text{ }^\circ\text{C}$) of voluminous sizes (up to 790 cm^3) which permit the use of natural samples and the insertion of thermocouples to monitor the evolution of temperature distribution during measurements. In selected experiments a sensor was connected to the upper piston to monitor acoustic emission associated with the generation of cracks within the melts as they cross the ductile-brittle transition.

A series of measurements on NIST standard material SRM 717a was initially performed to calibrate the instrument. The viscosity determined via Gent's equation was compared to certified viscosity data of the standard material. This work shows that the apparatus can resolve the viscosity of voluminous melt samples to within 0.06 logarithmic units. Several series of experiments were then carried out on natural samples with high-crystallinity (>50 %) to simulate dome lava deformation under various stresses and strain rates. Under eruptive conditions, dome lavas are non-Newtonian fluids characterized by an important component of shear thinning. Moreover a remarkably singular dependence of apparent viscosity (η) on strain rate ($10^{-6} \text{ s}^{-1} < \dot{\gamma} < 10^{-3} \text{ s}^{-1}$) yielded the following universal rheology law at eruptive temperatures ($850 \text{ }^\circ\text{C} < T < 1100 \text{ }^\circ\text{C}$):

$$\log \eta = -0.993 + 8974/T - 0.543 * \log \dot{\gamma}$$

Beyond strain rates of 10^{-3} s^{-1} , this equation fails as the brittle regime prevails; the melts suffer severe cracking, while showing dependences to both strain and strain rate. Continuous micro-seismic monitoring of the melts across the ductile-brittle transition revealed that below strain rates of about 10^{-4} s^{-1} lavas behave in a ductile manner and are essentially aseismic. As strain rates increase, a commensurate exponential increase in micro-seismic activity, accompanied by crack localisation is observed. Complete brittle failure occurred at strain rates approaching 10^{-2} s^{-1} . The evaluation of macroscopic failure using the acceleration of seismicity according

to the material failure forecasting method (FFM) yielded very accurate predictions after 4 seconds of deformation; that is, 8 seconds before complete failure.

This state-of-the-art apparatus enabled the first systematic rheologic and seismogenic measurements on highly crystalline dome lavas. The occurrence of shear thinning described here favours the localization of strain along the volcanic conduit margin and therefore the development of plug-like flow. The rheological results coupled to the seismicity further support the association of seismic swarms with seismogenic shear zones during eruptions. Given our observation that lavas may behave like their volcanic rock equivalent at high strain rate, careful monitoring of their seismicity should be coupled to failure forecast methods to successfully predict impending lava dome eruptions in volcanic crisis.

Zusammenfassung

Dom-Bildenden Eruptionsmodellen ermangelt es zurzeit an der fundamentalen Beschreibung durch die Rheologie und die Seismizität der blasen- und kristallreichen Laven. Speziell ist ein vertieftes Wissen über den Übergang von einem duktilen zu einem spröden Verhalten der Lava notwendig, um den Übergang vom effusiven zu explosiven Vulkanismus vorherzusagen. Eine neuartige Hochtemperatur-Uniaxialpresse wurde konstruiert, um die Rheologie und die Seismizität von silikatischen Schmelzen und magmatischen Suspensionen unter relevanten magmatischen Bedingungen, insbesondere im Bereich des spröd/duktile Übergangs, für vulkanische Systeme zu untersuchen. Die neue Presse kann in zwei Moden betrieben werden: bei konstanter Kraft (bis zu 300 kN), oder bei konstanter Deformationsrate ($\sim 10^{-7}$ and 10^0 s^{-1}) um Viskositätsexperimente im Bereich von 10^8 bis 10^{12} Pa durchzuführen.

Das rheologische Instrument ermöglicht erstmals Deformationsmessungen an homogen aufgeheizten ($\pm 2 \text{ }^\circ\text{C}$) und voluminösen Proben (bis zu 790 cm^3) von natürlichen Gesteinen bei gleichzeitiger Überwachung der Temperaturverteilung innerhalb der Probe. Dies ist u.a. zur Abschätzung des „Viskosen-Heizen-Effektes“ notwendig. Bei ausgesuchten Messreihen wurde zusätzlich ein akustischer Sensor an einem der Stempel angebracht, um die akustischen Emissionen während des Deformationsprozesses aufzuzeichnen.

Die Uniaxialpresse wurde mit Hilfe eines Viskositäts-Standard-Glases (NIST standard material SRM 717a) kalibriert. Die Viskosität wurde dabei durch die Gent-Gleichung bestimmt und mit den zertifizierten Werten des Standards verglichen. Die Messwerte stimmten innerhalb ± 0.06 logarithmischer Einheiten überein.

Anschließend wurden einige Messreihen an natürlichen, hochkristallinen ($>50 \%$) Proben durchgeführt, um die Verformung von Lava unter verschiedenen Drucken und Deformationsraten zu simulieren.

Unter eruptiven Bedingungen zeigen Dom-Laven ein non-newtonisches, rheologisches Verhalten. Die deformations- und temperaturabhängige, apparente Viskosität kann dabei durch ein universelles Gesetz im Bereich von $10^{-6} \text{ s}^{-1} < \dot{\gamma} < 10^{-3} \text{ s}^{-1}$, $850 \text{ }^\circ\text{C} < T < 1100 \text{ }^\circ\text{C}$ wie folgt beschrieben werden:

$$\log \eta = -0.993 + 8974/T - 0.543 * \log \dot{\gamma}$$

Bei höheren Deformationsraten $>10^{-3} \text{ s}^{-1}$ muss die Gleichung modifiziert werden. Im Übergang in den spröden Bereich treten zusätzliche Effekte auf.

Die Auswertung der mikroseismischen Aufzeichnung zeigte, dass Laven bei Deformationsraten von $< 10^{-4} \text{ s}^{-1}$ sich im Wesentlichen aseismisch verhalten. Bei höheren Deformationsraten wird ein exponentieller Anstieg der mikroseismischen Aktivität

beobachtet, die durch Konzentration von Rissen und Brüchen in der Schmelzmatrix und in den Kristallen hervorgerufen wird, bis es bei Deformationsraten von etwa 10^{-2} s^{-1} zum kompletten Makrobruch der Proben kommt. Die Evaluation des makroskopischen Versagens, kann durch die "material failure forecasting method" (FFM) nach 4-5 Sekunden des Deformationsgeschehens vorhergesagt werden. Also etwa 8 Sekunden vor der kompletten Zerstörung des Probenmaterials.

Die mit Hilfe der neuartigen, "state-of-the-art" Hochtemperatur-Uniaxialpresse gewonnenen Ergebnisse ermöglichen erstmals eine systematische, rheologische und seismische Untersuchung an natürlichen, hochkristallinen Proben. Das untersuchte non-newtonische Verhalten der silikatischen Schmelze in einem Vulkanschlot führt zu einer Stresslokalisierung innerhalb der Kontaktzone zwischen Magma und Nebengestein. Damit kann ein „Plug-Flow“ ausgelöst werden. Die rheologischen Ergebnisse zeigen darüber hinaus, dass auch von der unterkühlten, silikatischen Schmelze, seismische Signale ausgesendet werden können. Diese wurden bislang ausschließlich dem Zerbersten von Nebengestein zugeschrieben und ermöglichen bei Anwendung der "failure forecast method" die Vorhersage der Dom-Eruption bei aktiv überwachten Hochrisikovolkanen.

Munich, 14. November 2007

Dear Mountains Made Of Steam,

“The Earth is not a cold death place”
- Explosions in the Sky

Chapter 1

INTRODUCTION

Arc volcanoes commonly exhibit cycles of lava dome growth and catastrophic explosions. Lava domes are threatening since they act as plugs inside active volcanic craters like corks do for bottles of sparkling wine. Their cycle of growth and explosion leads to frequent, impulsive, and highly destructive volcanic disasters. For instance two thirds of the population of the island of Montserrat, in West Indies, has been evacuated since 1995 due to dome activity at Soufrière Hills (Avery, 2003). Fortunately, close monitoring and severe restrictions limited the fatalities to less than 10. Less lucky were however the 28000 inhabitants of St-Pierre in Martinique who were killed in 1902 by the collapse and explosion of a lava dome (Lacroix, 1902; Tanguy, 1994). Yet, today, nearly half a billion people live near an active volcano, and a serious effort is required to prevent such disasters to recur.

Nowadays, these active volcanoes are monitored by multiple geophysical and geochemical instruments which found our grounds in order to accurately forecast upcoming eruptions. Fortunately eruption precursors are numerous. However in the elaboration of eruptive scenarios, modellers find themselves facing a dead-end while the rheology, that is the flow behaviour, of the lava involved in these eruptions is as of yet very poorly constrained. Understanding the nature and efficiency of the physico-chemical processes involved in these eruptions is fundamental to risk assessment and hazard mitigation. A characterisation of the physico-chemical parameters controlling the rheology of lava domes is thus pressing and precisely the objective of this study.

1.1. lava rheology

Lavas and magmas are primarily silicate melts. In recent years much effort has been concentrated on the rheology of single-phase melts (i.e., crystal- and bubble-free lavas) under conditions relevant to volcanism. Especially the description of properties such as the temperature, pressure and chemical composition on melts' viscosity has been greatly improved (Bouhifd et al., 2004; Dingwell, 1998; Dingwell et al., 1998a; Dingwell et al., 1998b; Goto et al., 1997; Hess and Dingwell, 1996; Holtz et al., 1999; Scaillet et al., 1996; Schulze et al., 1996; Schulze et al., 1999; Stevenson et al., 1998; Stevenson et al., 1995). Experimental work showed that silicate melts are viscoelastic fluids behaving according to the classical work of Maxwell. Essentially, the melt behaves as a Newtonian fluid at low strain rates (that is the stress to strain rate relationship is linear and passes through the origin). However, as the deformation speeds up to near the relaxation timescale of the melt structure, a transition from a more viscous to more elastic response occurs and the rheology becomes non-Newtonian (that is the stress-strain rate relationship departs from the linearity). This change of behaviour is known as the glass transition temperature and it can be crossed by changing the strain rate or the temperature, or a combination of the two (Figure 1-1).

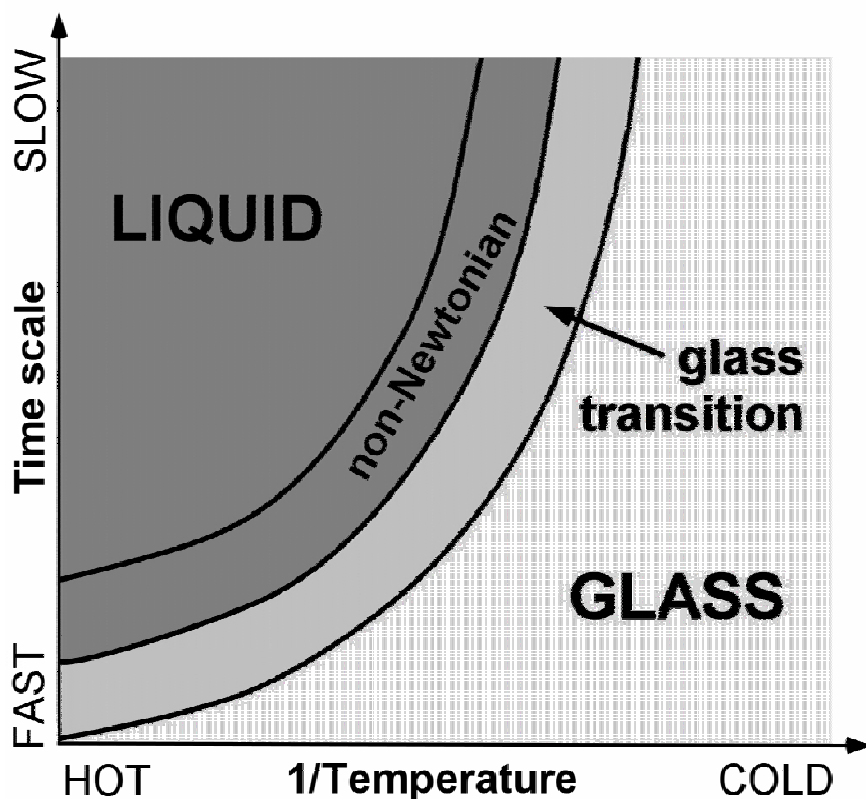


Figure 1-1. Sketch of the glass transition field. During slow deformations, or at high temperatures, melts are liquid behaving as Newtonian fluid. Upon temperature decrease or strain rate increase, liquids enter an unrelaxed state and become non-Newtonian fluids. Ultimately, they may become glasses if they cross to the brittle field (modified from Dingwell, 1996).

In nature, lavas inevitably contain a varied amount of crystals and bubbles and their rheology remains as of yet incompletely resolved (A detail account of the works on suspension applied to geological process can be found in Petford, 2003). Rheologists tackled the problem of suspension from both sides: by increasing the crystal content of a liquid, and by increasing the melt fraction of a rock. Einstein (1606, 1911) and later Roscoe (1952) derived equations to quantify the relative viscosity (η) increase caused by the crystal fraction (0 to ~40%) in a Newtonian fluid (Figure 1-2):

$$\eta = \eta_0 (1 - \Phi/\Phi_m)^{-n} \quad (1)$$

where η_0 is the viscosity of the melt phase, Φ the crystal fraction, Φ_m is the critical packing of the crystals, and n is a constant considered as an adjustable parameter. This non-linear equation predicts an important viscosity increase as the crystal fraction approaches the critical packing value. Einstein first pointed the difficulty of using such a general equation while an increased crystal content (above as little as ~8%) will occasion common solid-solid collisions which drastically influence the suspension rheology. In such cases a departure from a simple Newtonian behaviour would result. The critical packing value is indeed critical here, as it corresponds to the geometry of the crystal which, depending of their shape, may impede flow to different extent. In geological system, the varied shape, size and mean size distribution of crystals complicate heavily this variable and therefore the use of such equations.

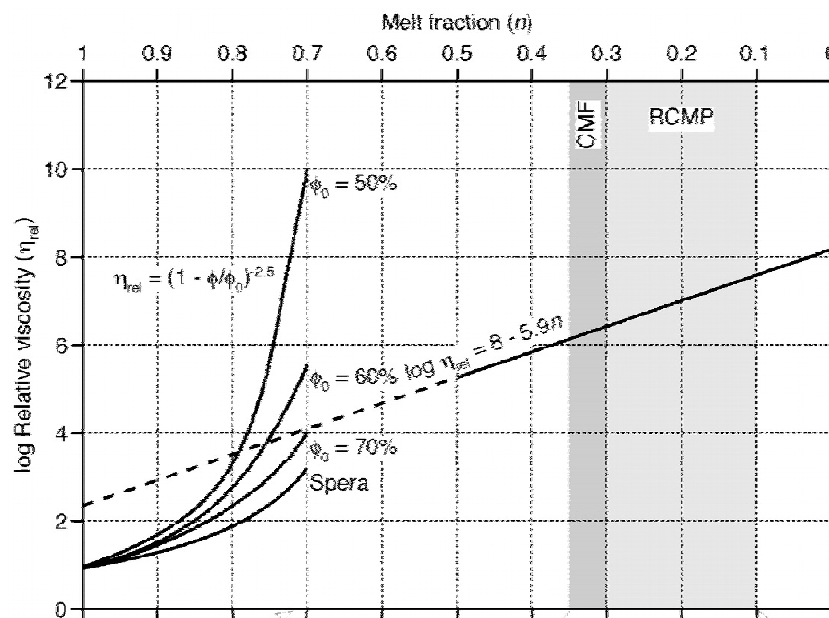


Figure 1-2. Effects of crystal fraction on the relative viscosity of a melt. The theoretical curves at low crystallinity were derived for critical packing values of 50, 60, and 70% (after Pinkerton and Stevenson, 1992; Spera, 2000). Solid line (and dash line extrapolation) refers to the work of Bagdassarov and Dorfman (1998) for a crystallinity of 50 to 100%. The RCMP and CMF are from Arzi (Arzi, 1978), and van der Molen and Paterson (1979). Diagram modified from Petford (2003).

Complementary work on partially molten rocks aimed at understanding the strength decrease associated with an increase in melt fraction (1978; Bagdassarov and Dorfman, 1998; van der Molen and Paterson, 1979). Although their work cared for the strength of molten rocks (and not viscosity), their findings revealed an important strength drop at around 25-30% melt which was named rheological critical melt percentage (RCMP; later termed critical melt fraction, CMF). Later works showed that two strength transitions actually exist: the first and most important strength drop actually occurs between 0 and 8% melt and relates to the wetting of crystal boundaries, while the CMF accounts for a much smaller strength decrease (for further discussion, refer to Rosenberg, 2004; Wickham, 1987). Nonetheless, the RCMP appears to be consistent with the abrupt viscosity increase observed near the critical packing value derived in the Einstein-Roscoe works; although strength and viscosity are concepts which cannot be directly compared.

Recent experimental work tried to track the viscosity jump across the CMF. Lejeune and Richet (1995) synthesized melts with defined contents of spherical particles, and performed low-load parallel plate experiments. Their work confirmed the uses of $\Phi_m = 0,6$ and $n = 2,5$, and the onset of the CMF around 40% crystals. It also points to the presence of yield strengths (~ 10 s kPa) above this crystallinity and the change to a non-Newtonian rheology. Costa (2005) used existing experimental data and empirically developed a set of equations to compute the apparent viscosity of melts with any crystallinity (0 to 100%). In accordance with experimental work of Lejeune and Richet (1995) and the theoretical work of Einstein and Roscoe, these new equations helped to outline of crystallinity rheology, yet they did not account for the strain-rate dependency of the suspensions.

Brückner and Deubener (1997) developed a phenomenological flow equation describing the strain rate effects on multiphase melts apparent viscosity (η_{app}).

$$\eta_{app} = \eta_{\infty} + (\eta_0 - \eta_{\infty}) (\gamma_g/\gamma) [1 - \exp(-\gamma/\gamma_g)] \quad (2)$$

Where η_{∞} is the ultimate Bingham viscosity when the strain rate (γ) is infinite, η_0 is the static Newtonian viscosity and γ_g is the flow relaxation rate. Such an equation poses a problem, Bingham conditions at high strain rates cannot be attained as the suspension fails long before. Yet this work specifies that an increase in crystal content will result in a stronger strain rate dependency of the viscosity.

Over the last hundred years, experiments, theoretical and empirical models attempted to portray the rheological properties of suspension. The difficulty of suspension lies in dealing with plasticity in the solid mechanic continuum and with a non-Newtonian fluid in fluid

mechanics. The novel work presented here treats both worlds and try to merge the field of rheology, volcanology and seismology to forecast volcanic eruptions.

1.2. Seismogenic volcanic conduits

Seismograms are used to infer the occurrence of certain geologic processes. In active volcanic area, volcano-tectonic earthquakes are frequent, yet; two types of seismic signals are most commonly related to eruptions (Burlini et al., 2007). (1) High frequency seismic events produce high amplitude P- and S-waves with frequency ranging from 5 to 15 H. This seismic activity is a precursor to the initiation of an eruptive phase and often occurs as swarm. (2) Low frequency earthquakes (also known as long period earthquake or LP) produce emergent P-waves, weak S-waves and they have frequencies ranging between 0.1 and 3 Hz. LP and volcanic tremors generally coincide with the occurrence of an eruption. While much controversy remains as to the processes causing these signals, it is generally accepted that they originate within the magma inside the eruptive conduit.

Recent field work on eroded shallow volcanic conduit uncovered a much complicated rheological dynamics. Structural and textural evidences revealed the common existence of seismogenic fault zones in which multiple cycles of rupture, slip and healing have occurred in the magma due to temperature and strain rate variations across the glass transition (Figure 1-3) (Tuffen and Dingwell, 2005; Tuffen et al., 2003). Tensile cracks entwined with shear bands are common along conduit margins (Figure 3b, Tuffen and Dingwell, 2005). A complex structure of pulverised glass and broken crystals known as tuffisite veins is often observed in these tensile cracks. These textures are very similar to the seismogenic fluidization of cataclasite in fault zones. It was proposed that cataclasite may be triggered by acoustic energy release during rupture (Melosh, 1996). Similarly the formation of tuffisite veins in magma stands as a plausible mechanism for the generation of low-frequency seismic events recorded during volcanic eruptions (Kumagai and Chouet, 2000). Complementarily, the absence of S-wave arrivals in hybrid earthquakes is consistent with a source within flowing magma, rather than solidified rock (Neuberg, 2000; White et al., 1998). The increasingly widespread observation of complex shear bands between the country rocks and the magma thus appears to portray a volcanic conduit which may be smaller physically as it is chemically. In other words, even though the magma chemically extends out till the crystallized country rock, the portion of magma contributing to the eruption dynamic is delimited by the seismogenic shear zones, which are dictated by the shear rate to structural relaxation timescale relationship. In

this scenario, the locations of crack propagation therefore play a major role in the triggering of explosive eruptions.

a



b

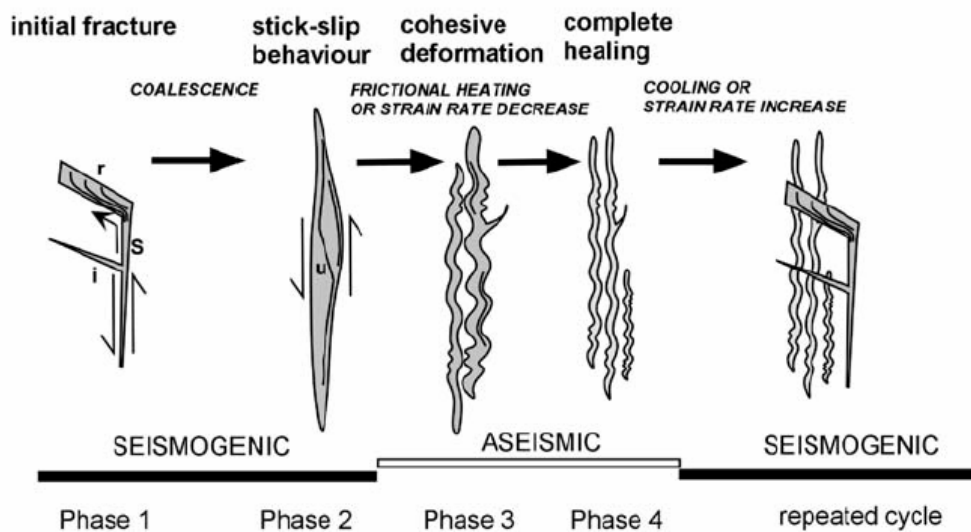


Figure 1-3. Repeated fracture and healing cycles. (a) Example of entwined ductile and brittle textures in a volcanic rock from Unzen (Japan). (b) Schematic view of seismogenic cycles of fracture and healing within rising magma. s corresponds to fault vein, i to injection vein, r to reservoir zone, and u to ultracataclasite zone.

1.3. Acoustic Emission (AE)

The experimental generation of cracks in deforming rocks has been studied intensively through acoustic emission (AE) monitoring (e.g., Byerlee and Lockner, 1976; Cox and Meredith, 1993; Dobson et al., 2004; Knillj et al., 1968; Koerner et al., 1981; Lockner and

Byerlee, 1977; Main et al., 1993; Meredith et al., 2001; Ohnaka, 1983; Ojala et al., 2004; Prikryl et al., 2003). AE generated by microcrack growth are used to track the development of macroscopic failure, since their temporal, spatial and size distribution follow a power law akin to earthquakes (Ojala et al., 2004). AE are high-frequency strain waves analogous to low-frequency seismic waves in nature (Dobson et al., 2004).

Yet, AE were never used to characterize lavas even though they were suggested to provide “a sensitive procedure for monitoring the nature of the creep deformation” (Chmelik et al., 2002). It seems obvious from our knowledge of the viscoelastic nature of lavas, that AE should provide invaluable information to characterize the non-Newtonian regimes across the ductile/brittle transition; from its onset at low strain rate to its failure at high strain rate. In such cases, the data could be used to test whether eruption forecasting models can predict the catastrophic explosion of lava domes.

1.4. Failure Forecast Method (FFM)

Following the observation that lava extrusions are often preceded by an acceleration of seismic activity, Tokarev (1963) first proposed a method to forecast eruptions from the accelerating Benioff strain (square root of seismic energy). Voight (1988; 1989) then devised a more empirical method known as the material failure forecasting method (FFM) where the accelerating rate of precursory phenomena (e.g., hit count, released energy) correlates to the likelihood of failure- in this case, of an eruption:

$$\frac{d^2\Omega}{dt^2} = A \left(\frac{d\Omega}{dt} \right)^\alpha \quad (3)$$

where $d^2\Omega/dt^2$ and $d\Omega/dt$ are the acceleration and rate of the phenomenon being monitored. A and α are parameters to be determined, and more explicitly α is expected to evolve from 1 to 2 before an eruption (Cornelius and Voight, 1995). De la Cruz-Reyna and Reyes-Davila (2001) modified this approach (using a Kelvin-Voigt body) and tentatively matched all existing seismic data from two eruptions at Volcán de Colima, Mexico (Figure 1-4). Although their method was poorly constrained (and mainly a fit of infinite series of viscoelastic elements), it yielded reasonable agreements nonetheless. Kilburn (2003) described the fracturing time series that arise from random energy fluctuations within a finite volume subject to a constant remote stress and developed the multiscale fracturing method (MFM). He finds that the peaks in event rate (rather than all seismic events) describes best the path to failure and also confirms the use of $\alpha = 2$ when approaching failure. The previous equation can thus be simplified to:

$$\frac{1}{d\Omega/dt} = A(t_f - t) \quad (4)$$

Where t_f is the time expected at failure. Since the acceleration increase before failure, the extrapolation of the inverse rate to 0 should provide the time of failure. Empirically derived from the field of rock mechanics, this approach does not yield well-constrained forecasts of lava extrusions and explosions. This study thus aims to test that macroscopic failure of multiphase lavas at high strain rate can be predicted by the FFM.

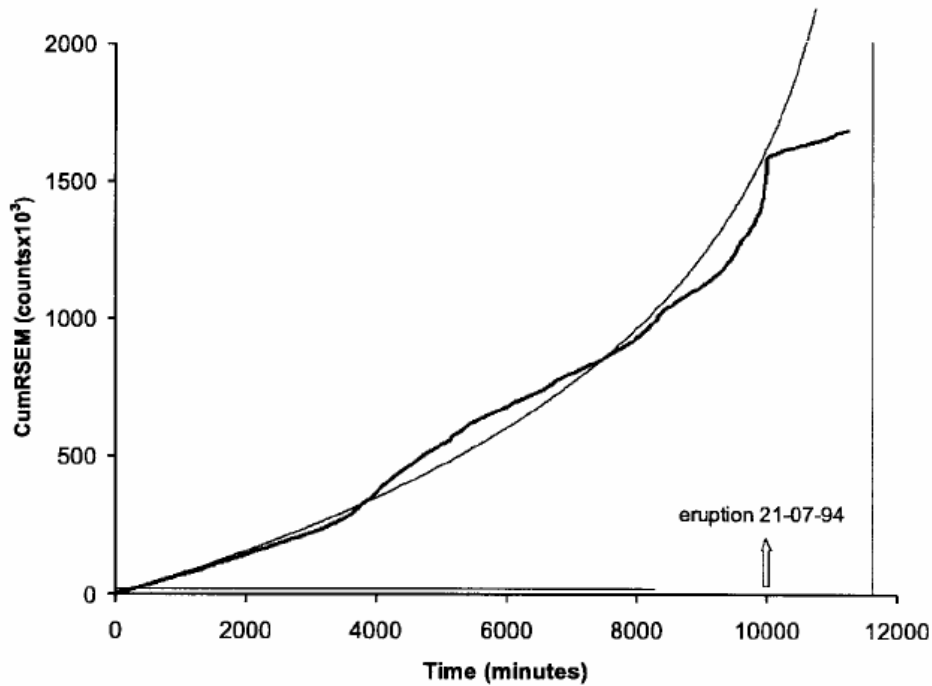


Figure 1-4. Eruption forecast based on the acceleration of seismicity. The heavy curve shows the cumulative counts of seismic event while the thin curve depicts the prediction of the model based on the first 8300 minutes. The model poorly predicts an eruption at 11627 minutes, that is one day after the occurrence of the actual eruption at 10000 minutes (from De la Cruz-Reyna and Reyes-Davila, 2001).

1.5 Uniaxial compression experiments

Following the theoretical work of Gent (1960) on the viscosities of cylindrical melt bodies deformed in compression, parallel plate apparatus were developed to study high-viscosity melts (Bagdassarov and Dingwell, 1992; Fontana, 1970; Lejeune and Richet, 1995; Neuville and Richet, 1991) Yet to experiment on natural material in which the crystals are abundant and large, a very large press was needed to avoid scaling ratio issues. Investigating

the rheological and seismological properties of multiphase melts thus required cutting-edge technology which was hitherto unavailable.

To achieve this task, a large high-pressure, high-temperature uniaxial press was developed and calibrated, and a series of rheological and seismological experiments were performed. The objective is to (1) provide accurate viscosity data at a range of pressure and temperature relevant to dome-building eruptions; (2) evaluate the rheology, and (3) describe the seismogenic character, of multiphase melts across the ductile-brittle transition; and (4) test whether the FFM can be used to accurately predict macroscopic failure of multiphase lavas.

“Hit me or kick me or hold me or please believe”

- A silver Mt. Zion Memorial Orchestra
and Tra-la-la Band

Chapter 2

HIGH-LOAD, HIGH-TEMPERATURE DEFORMATION APPARATUS FOR SYNTHETIC AND NATURAL SILICATE MELTS

A unique high-load, high-temperature uniaxial press was developed to measure the rheology of silicate melts and magmatic suspensions at temperature up to 1050 °C. This new apparatus is designed to operate at constant stresses (up to 300 kN) or constant strain rates ($\sim 10^{-7}$ and 10^0 s^{-1}), and further allows us to carry on experiments on samples with high viscosities ($\sim 10^8$ and 10^{12} Pa s). The rheological instrument represents an advance in that it accommodates homogeneously-heated samples ($\pm 2 \text{ }^\circ\text{C}$) of voluminous sizes (up to 790 cm^3) which permit the insertion of thermocouples to monitor temperature distribution evolutions during measurements. At last this setup allows for accurate measurements of viscosity of natural multiphase materials at strain rates and temperatures common to natural systems. The apparatus aspires to precisely (1) describe the onset of non-Newtonian behavior and its evolution with increasing strain rate until the point of rupture in the brittle regime, (2) constrain the effect of crystals and bubbles on the viscosity, and (3) record heating dissipated through viscous deformation. Here, a series of measurements on NIST standard material SRM 717a was conducted to calibrate this state-of-the-art apparatus. To this end, the viscosity determined via Gent's equation is compared to the certified viscosity data of the standard material. This work shows that the viscosity of voluminous melt sample can be resolved within 0.06 logarithmic units, and furthermore presents the detection of minor viscous dissipation for a high-temperature, high-strain-rate experiments.

2.1. Introduction

Many techniques have been used to quantify single-phase melts viscosity and their temperature, pressure, and compositional dependences (Ryan and Blevins, 1987). Magmas, however, inevitably contain some crystals and bubbles and the description of their influences on the rheology remains far from complete (Petford, 2003). Parallel plate technique was used to study the suspension rheology of silicate melts containing small particles (Lejeune and Richet, 1995), but the large size of crystals and bubbles in natural suspension, and its need to overcome a yield strength of 10s of kPa in order to flow (Petford, 2003), call for the fabrication of a larger apparatus capable of dealing with this material.

A unique high-load (<300 kN), high-temperature uniaxial press was developed to measure the rheology of silicate melts and magmatic suspensions at temperature up to 1050 °C. This new apparatus is designed to operate at constant stresses (~ 20 to 350^+ MPa) or constant strain rates ($\sim 10^{-7}$ and 10^0 s $^{-1}$), and further allows us to carry on experiments on samples with high viscosities ($\sim 10^8$ and 10^{13} Pa s). The rheological instrument represents an advance in that it accommodates voluminous samples height times larger than other currently available apparatuses. This permits the insertion of thermocouples to monitor temperature distribution evolutions during measurements. At last it will allow experiments on natural material at strain rates and temperatures common to natural systems (Manns and Bruckner, 1988; Quane et al., 2004). The range of experiments planned for this instrument especially aims at documenting rheological properties at relevant eruptive conditions. Measurements with this press shall thus extend the viscosity range investigated by Stein and Spera (2002), and describe melt rheology subject to stresses ((i.e., >50 MPa) higher than those of Quane et al. (2004). The apparatus essentially aspires to precisely (1) describe the onset of non-Newtonian behavior and its evolution with increasing strain rate until the point of rupture in the brittle regime, (2) constrain the effect of crystals and bubbles on the viscosity, and (3) record heating dissipated through viscous deformation.

The use of parallel plate measurements to study viscosity stem from the early work of Gent (1960) which derived the theory to calculate the viscous deformation of a cylindrical melt. Here, we present a series of measurements on NIST standard material SRM 717a and couple the viscosity determination using Gent equation with certified viscosity data of the standard to calibrate this state-of-the-art apparatus. This work shows that we can resolve the viscosity of voluminous melt sample within 0.06 log unit, and furthermore present the detection of minor viscous dissipation for high-temperature, high strain rate experiments.

2.2. Instrument design

A schematic illustration of the deformation apparatus is presented in Figure 2-1. The base unit consists of the load frame (Max Voggenreiter GmbH, Mainleus, Germany). Core of the press is a hydraulic CGS 280 servo cylinder with hydrostatic pocket bearings, which allows measurements in extension and compression. The system is equipped with a linear variable differential transducer LVDT (incorporated in the servo cylinder; travel range 150 mm, resolution 0.001 mm) at the top of the upper piston and a load cell at the bottom of the lower piston (Lorenz Messtechnik GmbH, force sensor K11, range +/- 400 kN, accuracy class for tension or compression 0.05 %). It is capable of applying constant displacement rates from 0.005 up to 600 mm per minute (strain rates $\sim 10^{-7}$ to 10^0 s⁻¹ for samples with lengths of 10 to 100 mm) or working in a constant load mode up to 300 kN. The press accommodates cylindrical samples with a maximum length and diameter of 100 and 100 mm, respectively. Pistons are machined from a nickel base, high-temperature, high-strength alloy (Rene 41) with good oxidation resistance up to 1050 °C and are cooled at their ends during operation conditions. The servo-cylinder is controlled by the software package HCE-HCELAB-1X/Z01 (Bosch Rexroth AG, Lohr am Main, Germany) operated on a test bed electronic system SYS-HCE-2X (same company) equipped with a measuring amplifier ME50S6 (Hottinger Baldwin Messtechnik GmbH, Darmstadt, Germany).

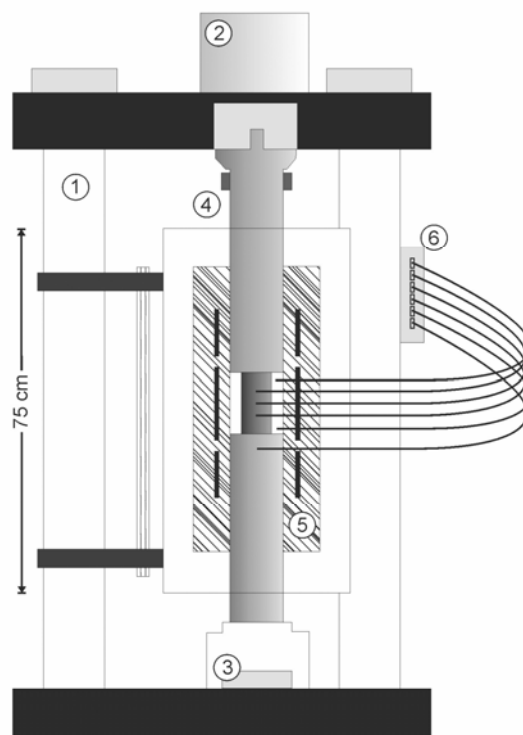


Figure 2-1. Sketch of the uniaxial press: (1) load frame; (2) servo cylinder with LVDT; (3) load cell; (4) cooling jacket; (5) 3-zone split cylinder furnace; and (6) 6-input thermocouple interface (for type K and S).

Attached to the load frame is a 3 zone, 12kW, split cylinder furnace (F-A 100-500/13_3, GERO Hochtemperaturöfen GmbH, Neuhausen, Germany) with CrFeAl-alloy heating wires operable up to 1100 °C. Thermal insulation is provided by a stiff fibre reinforced oxide ceramic SvM1514 (Walter E.C. Pritzkow Spezialkeramik, Stuttgart, Germany) in combination with flexible ceramic fibre blankets Alsiflex 1260 (Promat GmbH, Ratingen, Germany). Between 500 and 1050 °C, the three independent PID furnace controllers (Eurotherm 2704, Eurotherm Deutschland GmbH, Limburg an der Lahn, Germany) achieve a temperature stability of +/- 2 °C within a stable hot zone as long as 120 mm. At the highest temperatures, thermal equilibration of the system (piston and sample) occurs within 7 hours after a change in temperature.

The sample (enclosing up to three thermocouples equi-spaced alongside), the hot air zone and the lower piston temperatures are measured with shielded (Inconel) NiCr-Ni thermoelements (T.M.H., Hanau, Germany, Type K, D=1.5 mm) which can be read out by the six-input NI SCC-TC02 modules (National Instruments Corporation, Austin, TX, USA) built for conditioning signals from thermocouple types K and S. The modules include a 2 Hz lowpass filter and an onboard thermistor for cold-junction compensation and are fixed in a portable, shielded carrier (NI SC-2345).

Finally the deformation apparatus, the furnace, and the sample thermocouples are controlled and data acquisition is managed by a fast (sampling rate up to 333kS/s, 16-bit, PCI) NI 6052E PC-Card inside a standard PC in connection with LabView software (National Instruments Corporation, Austin TX, USA).

2.3. Parallel-plate-type viscosity measurements

Our calibration is done through a series of measurements on the NIST reference material SRM 717a as the exact viscosity can be predetermined using an equation valid for a wide range of temperatures (880 to 1555 °C). This standard material is advantageous as the large volume provided by the fabricant allows the preparation of large samples. Cylindrical core with a 2:1 height to diameter aspect ratio (40 x 20 mm) are prepared for this investigation. Three equispaced holes of 2 mm diameter are centrally drilled alongside the samples in order to insert three thermocouples and precisely monitor the temperature during the experiment. The sample is placed between the pistons and slowly heated up to a fixed temperature between 540-630 °C (we work in this low-temperature range to test-calibrate the press for high-viscosity measurements). After thermal equilibration, a pre-load is applied to get perfect parallel contact between the piston and the sample; then various loads (23-140 MPa) are applied until a maximum of 33 % strain is obtained [Note, these loads were applied

as calibration purposes since the viscosities remained in the Newtonian regime. This press is however designed to simulate higher stresses and investigate the onset and development of non-Newtonian behaviour in transition to the brittle regime]. The resultant length changes recorded by the differential transducer are then corrected for the instantaneous displacement undergone by the transducer itself upon applied pressure. The compliance of the piston was measured through a series of piston-piston load tests at different temperatures. Although very minor, this absorbed length changes (l) is understood according to:

$$l = 0.01691F^{0.6745} \quad (5)$$

where F is the force (N). The corrected values are then treated to obtain the corresponding viscosity.

The bulk viscosity of the melt (η in Pa*s) was calculated via the viscous equation developed by Gent for parallel plate measurements:

$$\eta = \frac{2\pi Fh^5}{3V\delta h/\delta t(2\pi h^3+V)} \quad (6)$$

where h is the length (m), and V is the volume of melt (m^3). We choose this equation which considers no-slip conditions as our deformed samples showed an absence or negligible amount of slip at the piston contact. The temporal profile of the viscosity is then refined via a spline smoothing algorithm.

2.4. Results on the NIST references material SRM 717a

A series of rheometric measurements were performed on the NIST SRM 717a (Table 2-1). The obtained viscosity profiles reveal mainly constant values of viscosities with time (or strain), which reflect the Newtonian behaviour of the melt under the tested conditions (Figure 2-2). Exceptions nevertheless arose for experiments at high temperatures and high strain rates, when slight viscosity decrease owing to viscous dissipation was monitored. Under the exerted conditions the obtained viscosity remained within error of the measurements, but it points to the importance of always monitoring the temperature distribution during viscosity measurements- especially for higher strain rate experiments in the non-Newtonian regime. A complementary investigation is currently undergoing which will serve to elucidate and model the extent of this viscous heating effect.

Table 2.1. Results for experiments on the SRM reference material 717a. ini: initial conditions; end: end conditions. For viscosity calculation purposes, the average temperature was used. Note the minor occurrence of viscous heating detected by any thermocouple between the initial and end measurements.

Run	Strain rate (s ⁻¹)	Stress (Pa)	Strain (%)	TC low (°C)	TC mid (°C)	TC top (°C)	T av (°C)	Viscosity Log (Pa*s) measured	Viscosity Log (Pa*s) calculated	Resid.
1-41-ini	1.9E-04	1.2E+08	11.2	540.61	541.60	538.23	540.15	11.29	11.40	0.11
1-41-end	1.5E-04	1.1E+08	15.9	539.99	540.71	537.57	539.42	11.31	11.42	0.11
2-27-ini	1.1E-04	8.1E+07	6.5	540.84	541.66	538.56	540.36	11.31	11.39	0.08
2-27-end	1.3E-04	7.9E+07	8.1	540.29	541.31	538.26	539.96	11.32	11.40	0.08
3-27-ini	1.3E-03	7.8E+07	9.1	569.89	571.96	568.45	570.10	10.27	10.29	0.02
3-27-end	1.2E-03	6.9E+07	20.4	569.84	572.07	568.59	570.17	10.25	10.29	0.04
4-10-ini	2.3E-03	2.8E+07	10.3	588.94	589.20	587.82	588.65	9.59	9.69	0.09
4-10-end	1.9E-03	2.3E+07	24.4	588.47	588.46	586.70	587.88	9.59	9.71	0.12
5-18-ini	6.0E-03	5.5E+07	4.5	594.01	594.69	591.98	593.56	9.49	9.54	0.05
5-18-end	5.0E-03	4.4E+07	23.6	596.94	598.18	594.09	596.40	9.41	9.45	0.04
6-16-ini	6.0E-03	5.0E+07	9.3	599.24	601.21	599.02	599.82	9.43	9.35	-0.08
6-16-end	4.8E-03	3.7E+07	32.2	600.42	602.98	600.11	601.17	9.33	9.31	-0.02
7-17-ini	1.6E-02	4.6E+07	12.5	613.75	615.16	613.36	614.09	8.98	8.95	-0.03
7-17-end	1.3E-02	3.7E+07	31.9	616.67	618.57	615.85	617.03	8.93	8.87	-0.06
8-10-ini	2.3E-02	2.7E+07	14.3	627.31	628.14	625.77	627.07	8.58	8.60	0.02
8-10-end	2.2E-02	2.5E+07	24.3	628.48	629.58	626.91	628.32	8.55	8.57	0.02

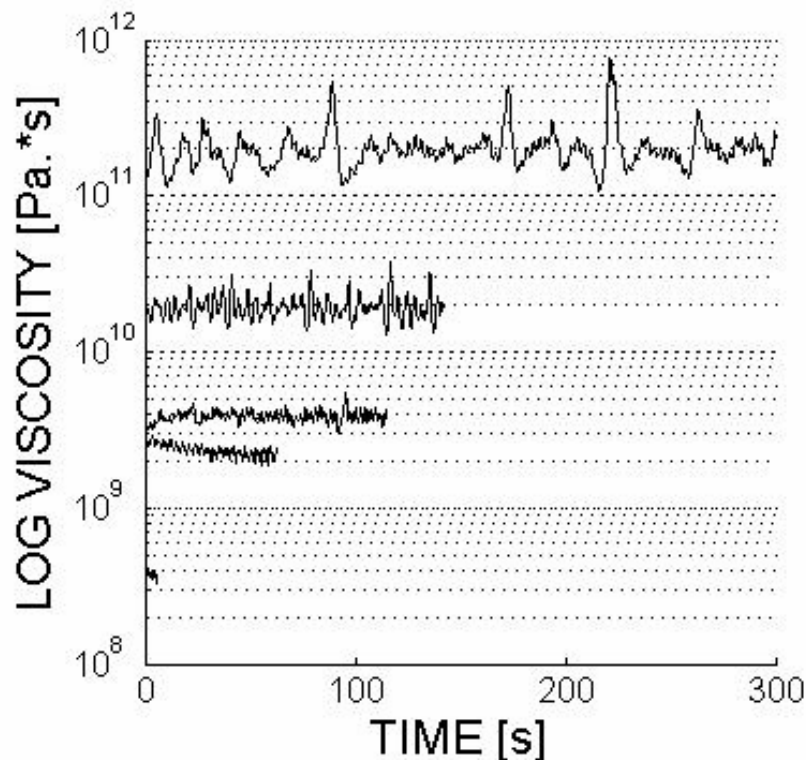


Figure 2-2. Viscosity data obtained for different initial conditions. Raw viscosity values are derived every 0.1 s.

Perhaps the most striking feature of this work is the excellent recovery we have between our viscosity measurements and the estimated values obtained via the certified equation (Figure 2-3); yet precise in spite of the large sample sizes. Our measurements

reproduced the viscosity to a precision of 0.06 log unit (Table 2.1); thus confirming the extension of the certified viscosity equation down to 540 °C. A slight offset to lower value can be observed at the high-viscosity end of the measurements but the values yet remain within the error of the measurement. Our results are furthermore in agreement with complementary measurements done in our lab with the micropenetration method on small-volume samples.

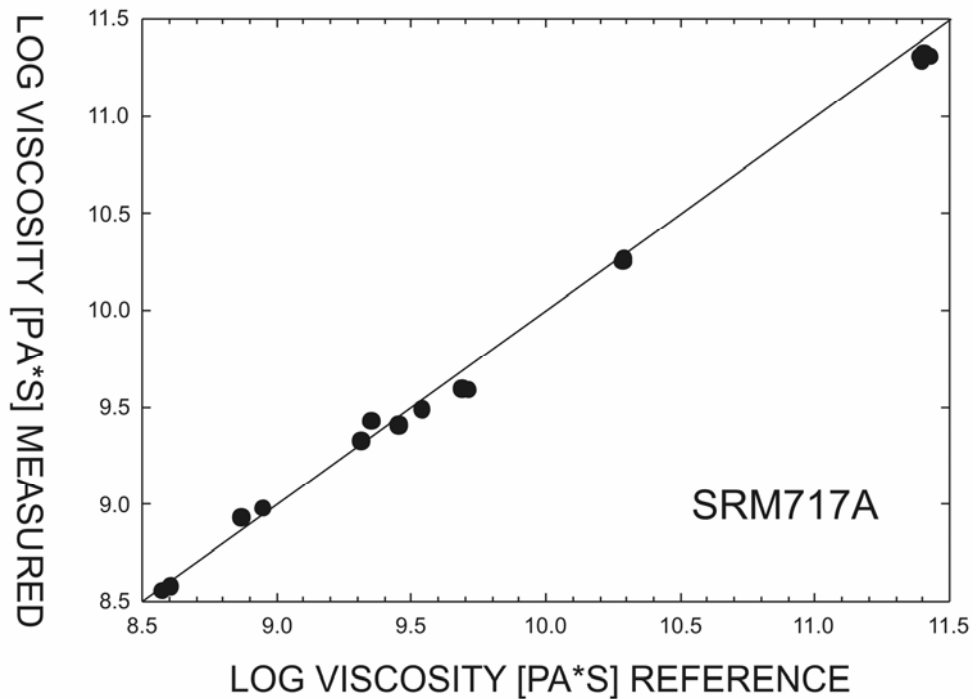


Figure 2-3. Obtained viscosity data compared to the certified values. The large data symbols span the error of the measurements. The 1:1 linear regression agrees to within 0.06 logarithmic units.

In retrospect we introduced here a new high-load, high-temperature deformation apparatus designed to sample at high data acquisition rate and thus to explore the non-Newtonian field of silicate melts with high precision and accuracy. The large size of the apparatus allow for the investigation of large samples in which we can insert thermocouples necessary in order to study viscous dissipation and the rheology of multiphase melts. The agreement obtained by this newly developed instrument is highly satisfactory and suitable to undertake viscosity measurements on large natural samples (Lavallée et al., 2007).

“In nature reality is selection
the tool of critical intervention
fragmentation is the rule
unity is not taught in school”

- Sonic youth

Chapter 3

NON-NEWTONIAN RHEOLOGICAL LAW FOR HIGHLY CRYSTALLINE DOME LAVAS

Volcanic eruption models are hampered by the lack of multiphase magmatic flow laws. Most rheological models estimate the viscosity of multiphase lavas via the Einstein-Roscoe equation, but this simplification cannot be used for high-crystallinity and it does not consider the non-Newtonian, strain rate dependence of viscosity. Here, experiments on natural samples using a unique high-load, high-temperature uniaxial apparatus were carried out to simulate multiphase lava deformation under various stresses and strain rates. Multiphase lavas exhibit an important component of shear thinning, and appear to invalidate the adequacy of Einstein-Roscoe-based formulations for highly-crystalline lava rheology. Indeed the remarkably singular dependence of viscosity (η) on strain rate ($\dot{\gamma}$) yields a novel, universal rheology law at eruptive temperatures (T):

$$\log \eta = -0.993 + 8974/T - 0.543 * \log \dot{\gamma} \quad (7)$$

This work reveals the importance of considering micro-cracking and viscous dissipation at very high strain rate ($>10^{-3} \text{ s}^{-1}$), thus explaining the occurrence of seismic swarms along the conduit margins, and consequently supporting plug-like magma ascent models.

3.1. Introduction

Understanding the nature and efficiency of physico-chemical processes involved in effusive and explosive volcanism is fundamental to risk assessment and hazard mitigation. Such processes are unfortunately not easily accessible or observables in actual eruptions. In the past, risk assessment has been chiefly relied on monitoring combined with numerical simulations. Recently however, advances in experimentation on natural materials at relevant temperatures and pressures has contributed to quantification and modeling of magmatic behavior in conduits and domes during eruption (Alidibirov and Dingwell, 1996; Kennedy et al., 2005; Spieler et al., 2004; Tuffen et al., 2003).

Accompanying this development is the fact that the description of single-phase melt properties such as the temperature, pressure and compositional dependence of viscosity has been vastly improved in the past decade (Giordano et al., 2006; Hui and Zhang, 2007). This combination of developments has advanced the physico-chemical basis of volcanic simulations in terms of mechanistic considerations and effective parameterizations greatly (Gonnermann and Manga, 2003; Melnik and Sparks, 1999; Papale, 1999a). Lavas, however, inevitably contain some crystals and bubbles and the description of their influences on the rheology remains far from complete (McBirney and Murase, 1984; Petford, 2003). In fact, observations from dome-building eruptions, in particular, reveal variable but very high levels of both vesicularity and crystallinity in erupting lavas.

In fluid mechanics, a suspension rheology is generally understood as a fluid in which the addition of particles increases the viscosity nonlinearly according to the Einstein-Roscoe equation (Einstein, 1906; Einstein, 1911; Roscoe, 1952). Problems with this expression nonetheless exist when extrapolating to particle concentrations greater than ~50% as the mixture becomes non-Newtonian and therefore strain rate dependent (Stevenson et al., 1996; Vigneresse and Tikoff, 1999). Suspension rheology studies on basaltic (Pinkerton and Norton, 1995; Ryerson et al., 1988), andesitic (Lejeune and Richet, 1995), rhyolitic melts (Alidibirov et al., 1997; Murase et al., 1985; Stevenson et al., 1996), and synthetic melts (Bruckner and Deubener, 1997; Deubener and Bruckner, 1997) at low to moderate stresses support this nonlinear increase of viscosity. Their findings seem to be consistent with an onset of non-Newtonian flow behavior at crystallinity greater than ~30%, and yield stresses of a few kilopascals (see discussion in Barnes, 1999). Furthermore, numerical models have emphasized that the extent of viscosity and yield stress increases across this transition depend on the degree of particle anisotropy and crystal size distribution (Saar et al., 2001). In this area, modeling volcanic eruptions is badly hampered by a paucity of data and, as a

consequence, the lack of an expression that describes the strain-rate dependence of the rheology of lavas hosting crystals and bubbles (Petford, 2003).

Here we investigated the rheology of natural melts subject to a wide range of stresses and strain rates. This study reveals important effects of strain rate on lava apparent viscosity and includes the generation of a general expression for the non-Newtonian regime of lavas with high crystal content.

3.2. Measurement method and viscosity determination

We used a high-load, high temperature uniaxial press to investigate the stress-strain rate behavior of multiphase lava (further details in Hess et al., in press). Here, cylindrical samples with a length to width aspect ratio of two (80×40 mm and 40×20 mm), and with a length at least ten times that of the largest crystal, were prepared for this study. This geometry minimized both edges and crystal-size scaling effects. The samples were inserted in the press and placed between two axial pistons which are surrounded by a three-zone furnace. The system was heated and equilibrated at high temperatures (940 to 1010 \pm 1.5 $^{\circ}$ C), then various loads (1–60 MPa) were applied to the sample until a maximum of 33% strain was obtained. Length changes of the sample were recorded at a rate of 10 times per second and the apparent viscosity of the melt (η_b in Pa*s) was then calculated via an equation developed by Gent (1960) for parallel plate measurements. Our calibration work demonstrated that we resolve the viscosity in Pa*s with an accuracy of \pm 0.06 log unit (Hess et al., 2007).

Four active volcanoes were selected for this study, namely Unzen, in Japan, Colima, in Mexico, Bezymianny, in Russia, and Anak Krakatau, in Indonesia (Table 3-1). The textures in the rocks were examined through microscopy and the open porosity of every sample was measured prior to, and after each experiment (Table 3-2). The samples for all volcanoes were highly degassed ($\leq 0.1 \pm 0.05\%$) and no volatiles were lost during the extensive heat treatment as confirmed by weight loss tests before and after treatment. The rocks chosen for this study cover wide ranges of geochemistry, crystallinity and vesicularity, and thus represent a significant portion of the range of lavas at active volcanic systems. We have used them to test the hypothesis that a simple non-Newtonian rheological law is capable of dealing with this range of materials, nonetheless.

Table 3-1. Normalized geochemical composition of 12 measurements on glass phase of each sample.

Oxides	Unzen	standard deviation	Colima	standard deviation	Bezymianny	standard deviation	Anak Krakatau	standard deviation
SiO ₂	77.77	0.32	73.18	1.18	75.26	0.63	64.60	0.81
Al ₂ O ₃	11.89	0.12	13.06	0.99	12.27	0.64	17.20	0.39
Na ₂ O	3.11	0.11	4.65	0.32	4.45	0.32	5.63	0.31
K ₂ O	4.65	0.12	3.73	0.39	3.72	0.51	1.74	0.18
MgO	0.08	0.01	0.37	0.20	0.19	0.05	0.65	0.53
CaO	0.68	0.19	1.40	0.59	1.30	0.41	5.14	0.69
TiO ₂	0.39	0.05	0.74	0.07	0.50	0.07	0.70	0.15
FeO	0.84	0.13	2.58	0.31	2.17	0.26	3.92	0.70
MnO	0.60	0.02	0.07	0.07	0.06	0.04	0.06	0.03
P ₂ O ₅	0.00	0.01	0.22	0.05	0.09	0.02	0.36	0.26
melt viscosity ¹ (Pa s)	10 ^{6.79}		10 ^{6.66}		10 ⁹		10 ^{7.25-8.8}	
bulk viscosity ² (Pa s)	10 ^{11.74}		10 ^{11.26}					

Note: The analyses were done with an electron microprobe, using a 15 kV, 20 nA scanning box mode (102 μm²). Standards: Si, Al and Fe: Ke-12 rhyolite; Na and Mg: albite; Ca: orthoclase; P and Ti: wollastonite; Mn: By-21; K and Ti: by-25. (1) Viscosity of the melt phase estimated at 940 °C after the work of Giordano et al.16 and Hess et al.8. (2) Viscosity of the bulk estimated via the Einstein-Roscoe equation for the melts with crystal content within the limit of the Einstein-Roscoe equation (see Table 1). Here we considered the ideal packing of 0.6 and the adjustable parameter value of 2.5 suggested by Lejeune and Richet (1995).

Table 3-2. Petrological and textural characteristics of rock samples.

Volcanoes	Glass (%)	Crystal (%)	Microlite (%)	Initial porosity (%)	End porosity (%)
Unzen	50	30	20	6	6
Colima	45	40	15	9	8.5
Anak Krakatau	30	55	15	23	21
Bezymianny	20	70	10	8	8

Note: The proportions of crystals, microlites, and glass (on a pore-free count) are averaged for 10 visual analyses coupled to digital estimates obtained via the JMicroVision 1.22 software. We resolved their proportion within 10%. The porosity of the sample were calculated by the Archimedian method and measured by a pycnometer. These porosities reflect an average of all samples, which did not vary by more than 1%.

3.3. Results

More than 40 experiments were performed to describe the influence of stress, and resultant strain rate, on the apparent viscosity of the multiphase lavas. At low applied stresses (<15 MPa) the initial deformation was characterized by a rapid nonlinear increase in viscosity until a steady value was reached (Figure 3-1). We associate this initial portion of apparent viscosity increase to the elastic responses of the press and sample upon application of stress. At intermediate stresses (~15–30 MPa) deformation occurred at a constant strain rate and the viscosity remained constant over the whole measurement (Figure 3-1). An instantaneous viscosity decrease was observed for each applied stress increment. At higher stresses (>30 MPa), the viscosity temporally decreased upon deformation; a delayed decrease of ~0.15 log unit occurred under a constant stress applied. In this rheological regime, the degree of delayed viscosity decrease was accentuated with increasing stress, and temperature increases

attributed to viscous heating began to be recorded by the thermocouple array (Figure 3-1). During these highest-stress experiments, the viscosity sometimes abruptly plunged and accompanying micro-cracking of the samples could be registered. Cracking of super-cooled melt results from high deformation rates which drive the system toward the brittle-ductile transition (Dingwell, 1996; Tuffen et al., 2003).

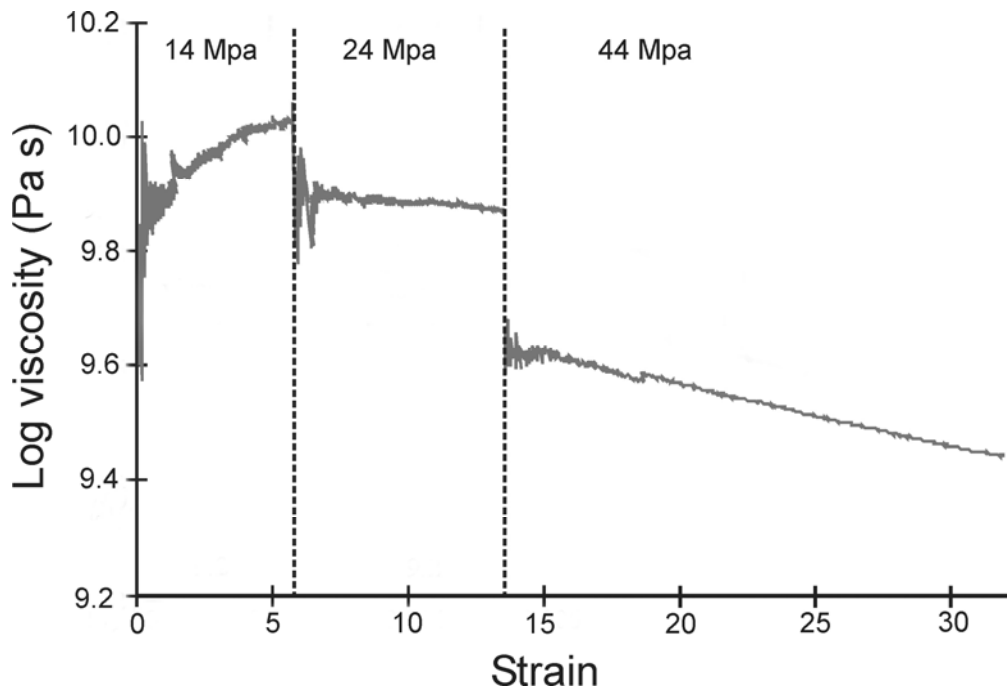


Figure 3-1. Typical viscosity profile for an experiment at 940 °C in which incremental stresses were applied. At 14 MPa, the viscosity nonlinearly increased with deformation due to elastic responses of the sample and the piston. At 24 MPa, the viscosity was constant throughout; however note the instantaneous decrease with respect to the viscosity at lower stress. A similar instantaneous drop can be noticed at 44 MPa, but here the high strain rate and accompanied viscous heating lowered the effective viscosity over the duration of the measurement.

Post-experiment textural analyses provide important complementary insights into suspension rheology. Upon deformation, the samples bulged laterally and extensional micro-cracks developed in periphery (Figure 3-2a). In the glass phase these cracks generally extend from one crystal to the next, whereas in the crystal phase the cracks seem to focus in the largest crystals primarily. We also notice a higher population of cracks inside the crystals for the experiments at higher strain rates. Even though cracks formed, some pores inside the melt closed and healed upon deformation; the end porosity values thus remained very similar to the initial porosity values, except for Krakatau samples in which the higher porosity lessened the occurrence of micro-cracking while allowing for more open pores to close (Table 3-2).

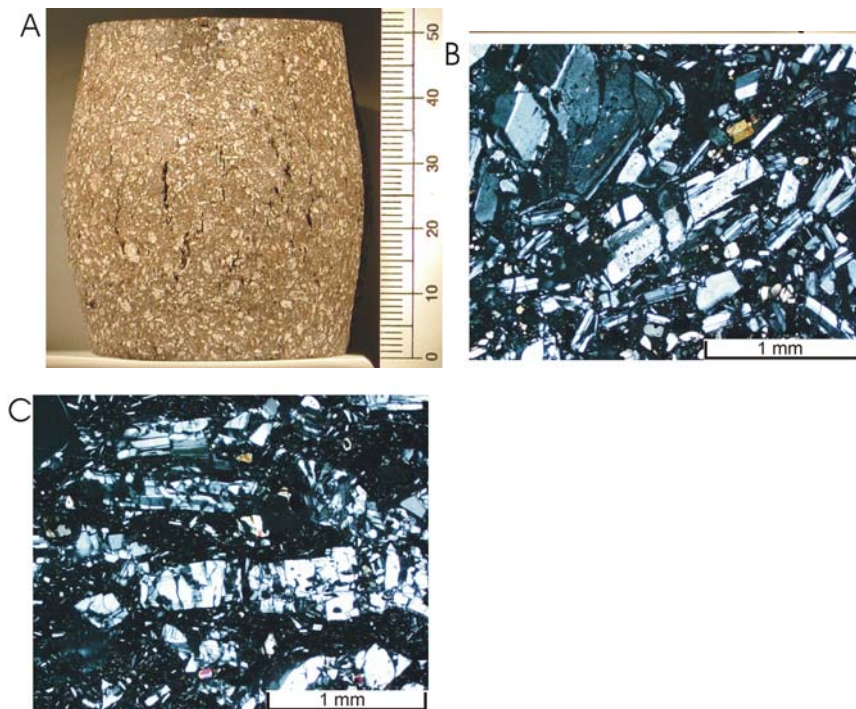


Figure 3-2. Post-experiment textures. (a) Bulging and minor lateral extensional cracking in a Colima sample deformed at 30 MPa. (b) Crystal re-orientation and alignment characteristic of ductile response of the suspensions at medium stress (vertically applied stress). (c) Crystal re-orientation and breakage due to brittle response of the suspensions at high strain rates (vertically applied stress).

Microscopic analysis also revealed a range of textures indicative of both viscous and elastic deformations. The alignments of crystals and melt into flow bands perpendicular to the applied stress evidenced the viscous response of the bulk in all samples and its dominant control on the obtained viscosity (Figure 3-2b). Otherwise, samples deformed at high strain rates were further characterized by multiple micro-cracks through phenocrysts (Figure 3-2b). In general these cracks were subparallel to the direction of stress, and restricted to the phenocrysts which had undergone rotation into perpendicular flow bands. At very high strain rates, micro-cracks were more closely concentrated and developed into longer fractures. The presence of large crystals sometimes deviated fracture propagation which showed their influence in changing the stress distribution. The micro-textural analysis showed the high importance of crystal organization in affecting the bulk of deformation and resultant non-Newtonian flow regime.

3.4. Singular non-Newtonian description of strain rate

The non-linearity between the applied stresses and resulting strain rates reveals that lava suspensions are pseudo-plastic fluids with a strong shear thinning component and

without any observable yield strength (Figure 3-3). The strain rate ($\dot{\gamma}$) can therefore be associated to the applied stress (σ) through a power law equation (Ostwald, 1925):

$$\sigma = k\dot{\gamma}^n \quad (8)$$

where k and n are the Ostwald and non-Newtonian constants, respectively (Figure 3-3). Interestingly the non-Newtonian parameter remains nearly constant for all samples, permitting the following simplification:

$$\sigma = k\dot{\gamma}^{0.51} \quad (9)$$

The accordance of the suspensions to a singular non-Newtonian constant is further reflected in the obtained viscosity data

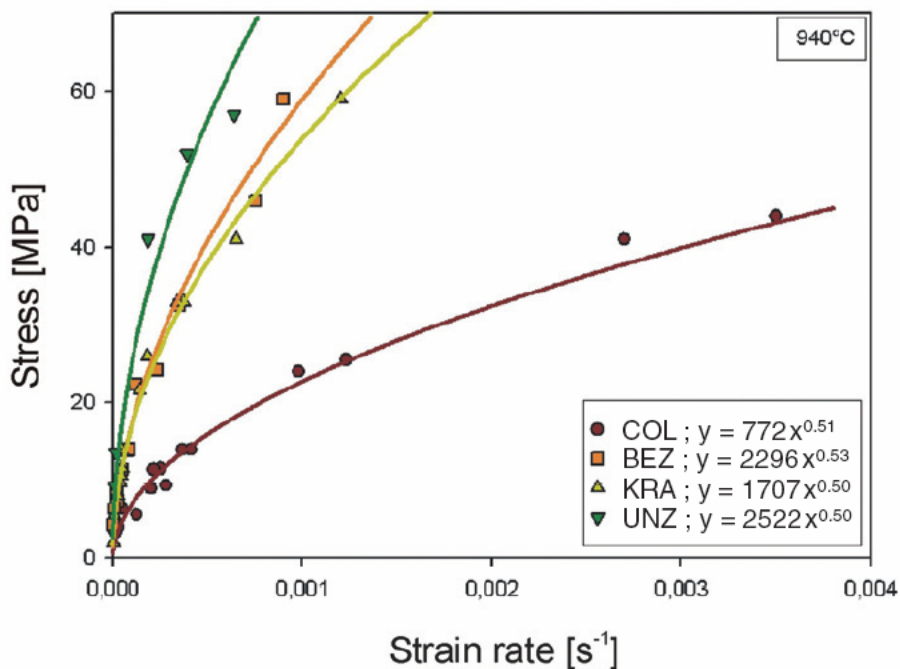


Figure 3-3. Stress-strain rate profile of experiments at 940 °C. Suspension lavas behave as pseudo-plastic fluids with a strong component of shear thinning of 0.510.

The results of all performed experiments reveal a linear relationship between the logarithms of viscosity and strain rate (Table 3-3; Figure 3-4). Interestingly and surprisingly, regardless of the volcano, and therefore the geochemistry, the crystal content, or the presence of 0–25% bubbles, all calculated viscosities equally decrease by 1.5 orders of magnitude by accelerating the strain rate from 10^{-6} to $\sim 10^{-2.5}$ s^{-1} ; point at which the strain rate began to speed up and the viscosity dropped under a given applied pressure. In contrast, single-phase melts at a similar viscosity are Newtonian up to $\sim 10^{-3}$ s^{-1} , that is their viscosity does not exhibit a dependence on the strain rate up to this limit where viscous heating lowers the viscosity (Hess et al., submitted). The viscosity/strain rate linear relationship and the deviation

from this main trend can thus be decoupled which ease our task to pinpoint different mechanical influences. Here we suggest that the presence of crystals causes the common, linear trend described whereas the deviation from this trend is an effect of micro-cracking and viscous heating which serves to increase the temperature of the interstitial melt and therefore decrease the viscosity further.

Table 3-3. Linear regressions for viscosity-strain rate data sets.

Volcanoes	T (°C)	a	b	Std. dev.
Colima	940	-0.518	8.297	0.063
Bezymianny	940	-0.543	8.584	0.038
Anak Krakatau	940	-0.545	8.597	0.036
Unzen	940	-0.565	8.735	0.057
Average	940	-0.543	8.553	
Colima	980	-0.519	7.905	0.000
Unzen	980	-0.493	8.653	0.042
Unzen	1010	-0.528	8.126	0.000

Note: T — temperature. Std. Dev.—standard deviation. The average of the linear regressions at 940 °C is displayed as the green line in Figure 4. The non-Arrhenian variations in temperature of the linear regressions (b values) were used as proxy to derive equation 3 and the blue and green lines of Figure 4.

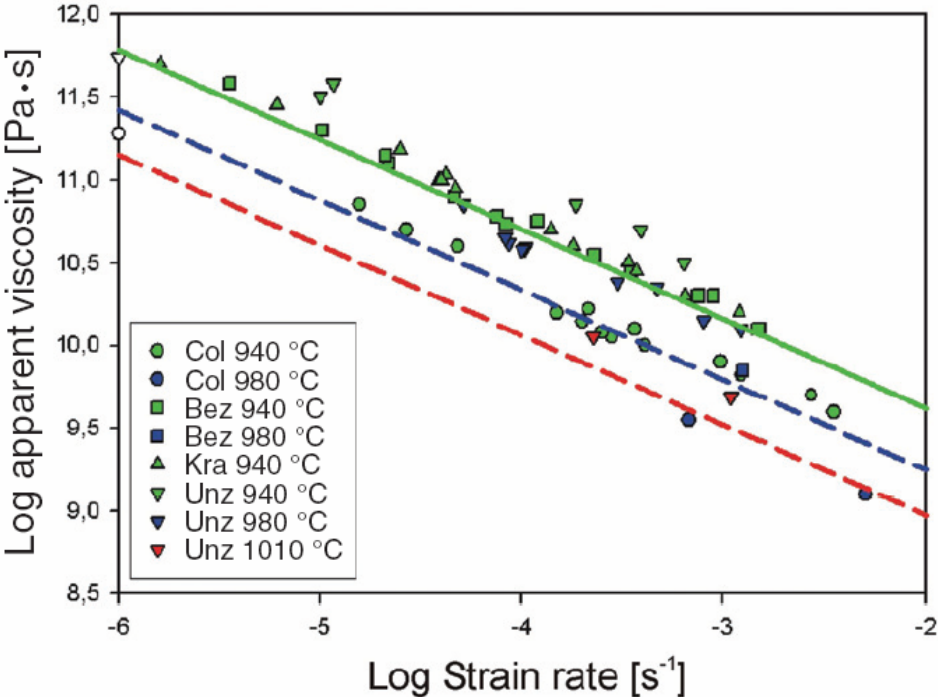


Figure 4. Viscosity-strain rate profiles for all performed experiments. The green line was modeled by averaging the best fit curves for each volcano at 940 °C (Table 3-3). The blue and red dash lines display the curves obtained through our general non-Newtonian rheological law (Equation 7) at 980 and 1010 °C, respectively. The viscosity estimates of Unzen (open diamond) and Colima (open circle) lavas plotted on the y axis were determined with the Einstein-Roscoe equation (see Table 3-2).

3.5. General non-Newtonian rheological law

The ubiquitous decrease in viscosity with increasing strain rate provides a valuable opportunity to refine our physico-chemical picture of eruptive flows. The range of apparent viscosities exhibited by the suspensions is mildly narrower than that of the interstitial melt viscosities obtained in previous work for pure melt phases within our temperature range (Table 3-1, Figure 3-4, Giordano et al., 2006; Hess and Dingwell, 1996). This suggests that for high-crystal content lavas (50–80%) the rheological regime is primarily dictated by the crystal phase while the importance of the interstitial melt viscosity is lessened. That observation implies, in turn, that with greater than 50% particles, suspension rheology equations such as the Einstein-Roscoe equation is, to a first order, irrelevant, for the description of these lavas as it overlooks their strain rate dependency.

The effect of strain rate is universal in this investigation, regardless of crystallinity or chemistry (see a and b parameters in Table 3-3). The strain rate dependency of viscosity was obtained by averaging the slopes (a) and intersections (b) of the linear regressions at 940 °C. We then followed Hess and Dingwell (1996) method and used the various b values of Unzen and Colima to parameterize the temperature dependence according to the well known non-Arrhenian behavior of silicate melts. Thus, a general expression capable of describing the non-Newtonian rheology of these lavas between ~850 and 1010 °C is provided by:

$$\log \eta_b = -0.993 + 8974/T - 0.543 * \log \gamma \quad (7)$$

where η_b is the apparent viscosity (Pa s), T the temperature (°C) and γ the strain rate (s^{-1}). It is important to stress that this is not a theoretical equation; it rather was entirely derived empirically and is only applicable when the vesicle content is below 25% and at moderate strain rates between $10^{-2.5}$ and $10^{-6} s^{-1}$. Yet this master equation described the entirety of our suspension viscosities within ± 0.2 log unit. We anticipate it will be highly effective in delivering insights into the modeling of magma ascent and volcanic eruption.

In a nutshell, the shear thinning exhibited by suspension lavas favors plug flow inside conduits (Ramos, 1999). At an active volcano such magma ascent dynamics is identified by the detection of periodic seismic swarms at a limited depth range along the conduit margin (Iverson et al., 2006; Rowe et al., 2004; Tuffen et al., 2003), and superficially expressed by dome growth or the extrusion of a spine. Plug disruption is known to produce catastrophic explosive eruption (Gonnermann and Manga, 2003; Papale, 1999b), but numerical models beg for better rheological constraints. Yet, the master equation and data presented herein strongly support recent modeling of stick-slip motion during the 2004–05 dome growth phase

at Mount St Helens (Iverson et al., 2006), and therefore will help merge the fields of volcanology, seismology, and numerical modeling in upcoming times of volcanic crisis.

In summary, the observed micro-textures and obtained viscosity data presented a new view on the rheology of lava containing 50%–80% crystals. Within this limit, the suspension obeys a simple linear regression which predicts its rheology up to strain rates of $10^{-2.5} \text{ s}^{-1}$. Above this strain rate, rheological models need to consider micro-cracking and heating generated by viscous dissipation. The simple equation non-Newtonian description of strain-rate dependent rheology proposed here should enable its easy incorporation in current volcanic eruption models. We anticipate that the result will greatly enhance understandings of volcanic flows.

“To turn up the signal, wipe out the noise”

- Peter Gabriel

Chapter 4

SEISMOGENIC LAVAS: FRACTURE AND ERUPTION FORECASTS

Volcanic dome-building episodes commonly exhibit acceleration in both effusive discharge rate and seismicity before explosive eruptions (Sparks, 2003). This should enable the application of material failure forecasting methods (FFM) to eruption forecasting (Kilburn, 2003; Voight, 1988). To date, such methods have been based exclusively on the seismicity of the country rock (Voight, 1989). It is however clear that the rheology and deformation rate of the lava ultimately dictate eruption style (Dingwell, 1996). The highly crystalline lavas involved in these eruptions are pseudoplastic fluids which exhibit a strong component of shear thinning as their deformation accelerates across the ductile to brittle transition (Lavallée et al., 2007). Thus understanding the nature of the ductile-brittle transition in dome lavas may well hold the key to an accurate description of dome growth and stability. Here, results of rheological experiments with continuous micro-seismic monitoring reveal 1) that domes lavas are seismogenic and 2) that the character of the seismicity changes markedly across the ductile-brittle transition. Below strain rates of 10^{-4} s^{-1} lavas behave in a ductile manner and are essentially aseismic. As the strain rate increases, an exponential increase in micro-seismic activity, accompanied by crack localization is observed. Complete brittle failure occurs at strain rates approaching 10^{-2} s^{-1} . Thus, molten lava may behave more like its volcanic rock equivalent than a fluid at these higher strain rates. These results demonstrate for the first time that lavas can be seismogenic. They contain the promise that magma seismicity, combined with FFM, can be applied successfully to dome-building eruptions for volcanic forecasting.

4.1. Introduction

Arc volcanoes commonly exhibit cycles of dome growth building up to catastrophic explosions, leading to dome collapse. Increasingly, these volcanoes are routinely monitored by multi-parameter (geophysical and geochemical) systems which provide a basis in practice for hazard management and forecasting of upcoming eruptions (Sparks, 2003). Fortunately for monitoring, precursory signals of volcanic unrest are common and numerous; yet their origins remain to be deciphered and properly characterised in mechanistic way. In particular, volcanic eruptions generate various types of seismic signals including continuous tremor and it is within the complexities of their waveforms that the description of the responsible internal processes (e.g., fluid oscillation, melt migration and fracturing) is likely to be found (Chouet, 1996; Harrington and Brodsky, 2007; McNutt, 2005; Neuberg, 2000; Neuberg et al., 2000). While many doubts remain as to the exact nature of volcano-seismic source mechanisms, it is nevertheless commonly accepted that brittle failure along the conduit margin can play a major role. To date, volcanic eruption forecasting models such as the material failure forecast method (FFM) assume that the seismicity originates from fracturing of the volcanic edifice (i.e., is not magmatic) (Voight, 1988; Voight, 1989). However recent fieldwork on eroded, shallow conduits has uncovered abundant evidence of a more complex magma rheology. In particular structural and textural evidence have revealed the common existence of seismogenic fault zones in which multiple cycles of rupture, slip and healing have occurred *in the magmas* due to strain rate variations across the glass transition (Tuffen and Dingwell, 2005; Tuffen et al., 2003). Elegant numerical models have further elucidated this shearing-induced fragmentation along the conduit walls; nevertheless, the implementation of these scenarios clearly awaits better rheological and seismological constraints (Gonnermann and Manga, 2003; Papale, 1999b).

Ultimately it is the competition between the strain rate and the relaxation timescale of a melt which dictates whether the eruption will proceed effusively or explosively (flow or blow) (Dingwell, 1996). Classically, a pure, single-phase melt behaves as a Newtonian fluid at low strain rate, but as the deformation speeds up to near the relaxation timescale of the melt structure, the melt becomes non-Newtonian. Viscous heating and microcracking ensue (Hess and Dingwell, 1996; Webb and Dingwell, 1990). In nature, dome lavas inevitably contain a variable amount of crystals and bubbles, yet their rheological influence remains incompletely resolved (Petford, 2003). Recent experimental and theoretical studies have helped in defining a realistic view of their non-Newtonian behaviour (Caricchi et al., in press; Cordonnier et al., Submitted; Costa, 2005; Lavallée et al., 2007). Nevertheless their complex mechanical state

involving components of fluid and solid behaviours denies us a complete constitutive relationship to date. Essentially, three rheological effects have been recognized as the strain rate (or stress) is increased (Cordonnier et al., Submitted; Lavallée et al., 2007). (1) An instantaneous viscosity decrease, recoverable upon stress release, defines multiphase lavas as a viscoelastic, or pseudoplastic fluid with a strong component of shear thinning. As the strain rate is further increased, the viscosity becomes strain dependent where a delayed decrease in viscosity is caused by (2) minor viscous heating and (3) audible cracking. This late cracking of lavas as it embraces the brittle regime may hold the key to forecasting lava dome eruptions.

The experimental generation of cracks has been studied extensively in the field of rock mechanics (Dobson et al., 2004; Ojala et al., 2004; Prikryl et al., 2003). Acoustic emission (AE) generated by microcrack growth are used to track the development of macroscopic failure, since their temporal, spatial and size distribution follow a power law akin to earthquakes (Ojala et al., 2004). AE events are high-frequency strain waves analogous to low-frequency seismic waves in nature (Dobson et al., 2004). Yet, AE has seldom been used to characterize deformation of lavas even though it has been proposed to provide “a sensitive procedure for monitoring the nature of the creep deformation” (Chmelik et al., 2002). The viscoelastic deformation described in our previous work is comparable to creep deformation (Lavallée et al., 2007). Here we use AE for the first time to characterize the acoustic character of the non-Newtonian regime of dome lavas across the ductile-brittle transition – from its onset at low strain rate to its failure at high strain rate – and to evaluate the failure prediction capability of the FFM.

4.2. Method and calibration

The experimental arrangement for this investigation couples two now well-established techniques. Firstly, a well-calibrated, high-load, high-temperature uniaxial press was used to study the effects of stress and strain rate on the apparent viscosity of lavas from Colima (Mexico) and Bezymianny (Russia) volcanoes (see Chapters 2 and 3). Secondly, a fast AE monitoring system was close-coupled to the press, and used to record AE output simultaneously and continuously during each deformation experiment (Figure 4-1).

Brittle failure during deformation was recorded by a computer developed by Physical Acoustics Corporation. AE generated by each crack increment produced a wave packet, or a hit. The AE sensor was positioned at the extremity of the upper piston which was used as a waveguide. For the purpose of the present study we used a WD broadband sensor operating between 100 and 1000 kHz with a peak sensitivity at 55 V or -62,5 dB. Used in a differential

mode, the sensor connected to a PCI-2 AE computer via preamp set at a 40 dB gain. The computer equipped with the AEwin™ real-time acquisition software acquired all incoming data and enabled replay and post-experiments analyses.

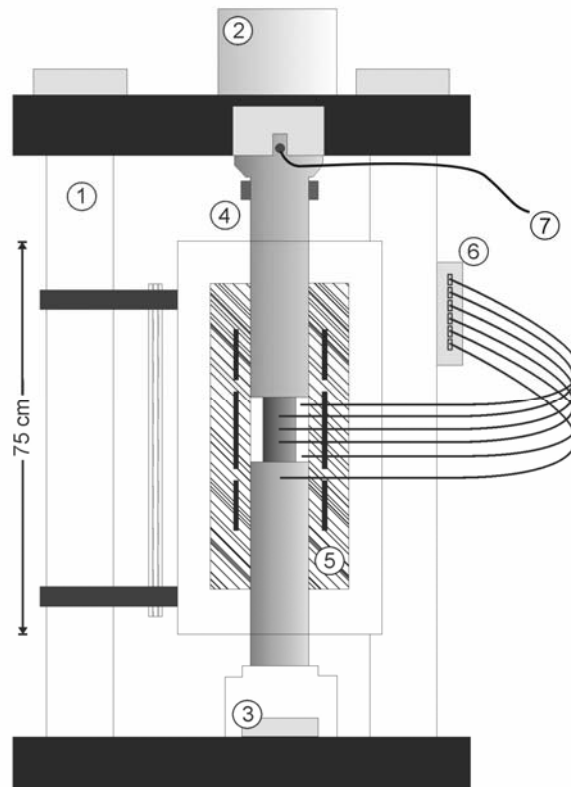


Figure 4-1. Sketch of the experimental setup. The high-load, high-temperature uniaxial press consists of a: (1) load frame; (2) servo cylinder with LVDT; (3) load cell; (4) cooling jacket; (5) 3-zone split cylinder furnace; and (6) 6-input thermocouple interface (for type K and S). The AE sensor (7) was glued to the cool, upper end of the piston and connected to PCI-2AE computer.

Preliminary tests were performed to assess the background noise generated by the uniaxial press, its hydraulic system and the surrounding heating furnace. We ran piston-to-piston deformation tests and purely viscous melt deformation on NIST standard material SRM 717a. Fortunately, our apparatus and setup produces little noise, which was nearly completely eliminated through the addition of a detection threshold at 50 dB. The second noise source was distinct and thus easily filtered out as it is produced by the hydraulic system during the transitional ramps to higher load. During these loading ramps which last six seconds, the press produces a peak of noise around 70-80 dB which (at stresses below 20 MPa) last up to ten seconds. The one remaining background noise was sporadic and could not be filtered (Figure 4-2). Generally of low amplitude (< 54 dB), a few hits recurred in average 13 times per

millimetre of deformation. Even though some of these events reached (76 dB), we judged them insignificant as (1) they were single peak hit unaccompanied by a tail of lower amplitude hits, and therefore (2) with an incoherent B-value, and because (3) the absolute energy produced was generally 1-2 orders of magnitude lower than events for multiphase melt deformation.

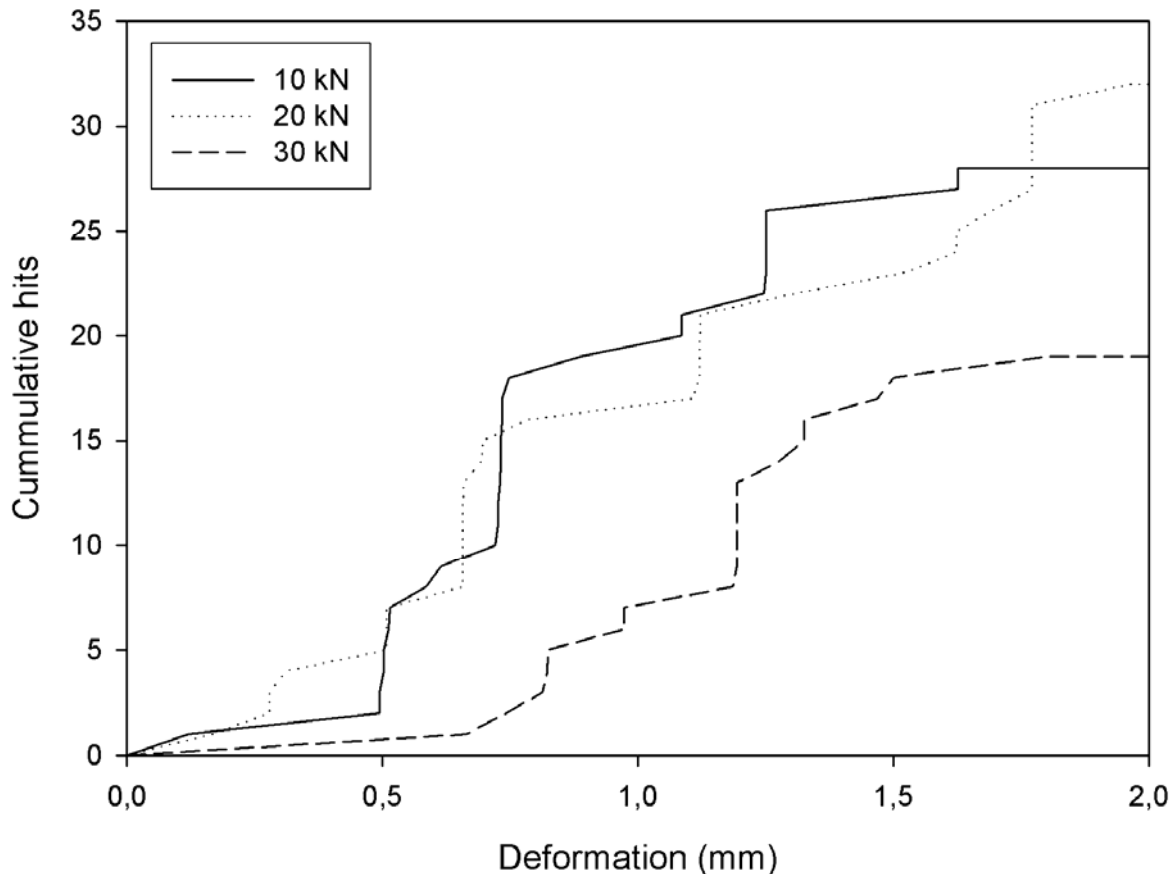


Figure 4-2. Background noise calibration experiments. AE hits recorded during deformation of the NIST reference material 717a, used to calibrate the noise of the uniaxial press.

We chose volcanic rocks from dome-building eruptions at Colima, in Mexico, and Bezmyianny, in Russia, because extensive experimental work was performed on them (Cordonnier et al., Submitted; Kueppers et al., 2006a; Kueppers et al., 2006b; Lavallée et al., 2007; Mueller, 2007; Mueller et al., 2005; Mueller et al., 2004; Richard et al., 2006; Scheu et al., 2007; Spieler et al., 2004). The textures in the rocks were examined through microscopy and the open porosity of every sample was measured prior to, and after each experiment.

At Colima, we collected dense lava dome blocks from a lahar deposit. The rocks are dacite with ~50 to 60 % of commonly euhedral crystals up to 2.5 mm in length. The

microlites showed minor signs of flow alignment. A dacitic lava dome block was similarly sampled at Bezymianny, but the phenocryst (up to 2 mm) and microlite contents reach ~80 %, and they are generally anhedral and mechanically eroded. Unlike inside Colima's dome rock the microlites at Bezymianny are more randomly interlocked and show no textural fabrics. The samples for both volcanoes were highly degassed ($\leq 0.1 \pm 0.05$ %) and no volatiles were lost during the extensive heat treatment as confirmed by weight loss tests before and after treatment. The rocks chosen for this study cover wide ranges of geochemistry, crystallinity and vesicularity, and thus represent a significant portion of the range of lavas at active volcanic systems. Experiments were performed under stresses of 1-40 MPa and temperatures of 900-980°C, *i.e.* under P-T conditions of dome-building eruptions.

4.3. Seismogenic profile across the ductile to brittle field

Viscosity profiles for multiphase lavas deforming under successively increasing increments of stress have been described recently (Lavallée et al., 2007). Here we extend that work to include the associated AE energy released by microcracking during deformation (Figure 4-3). Multiphase melt deformation under low stress (8 MPa) is typically characterized by a strong elasticity and thus a viscosity which increases at a decreasing rate until it stabilizes at a high, constant value (Figure 4-3A). Under these low stresses, no viscous heating is generated and the temperature remains constant (Figure 4-3B). A moderate number of AE is recorded during the viscosity increase, but with time the AE rate decreases to close to zero as viscosity stabilizes. Since the AE events are generally of low amplitude, the cumulative AE energy also remains low (Figure 4-3C). At intermediate stresses (16 MPa), the viscosity is often observed to remain relatively constant over the duration of the deformation, and minor viscous heating increases the temperature by about 0.5 °C (Figure 4-3A,B). Under this regime AE energy production rate also remains essentially constant (Figure 4-3C) but with occasional higher energy signals. Finally, at high stress (24 MPa), the viscosity decreases markedly during deformation (Figure 4-3A). This extreme regime is characterized by a noticeable degree of viscous heating and an accelerating output of AE energy (Figure 4-3B,C). Overall, the increase in AE energy with increasing stress is due both to an increase in the number of events and to an increase in individual event amplitude (*c.f.*, earthquake magnitude). This is, in turn, manifested in a decrease of the seismic b-value (slope of the cumulative number of events vs. amplitude) from >3.5 to as low as <1.5 in some cases. This observation implies a change from more distributed small-scale cracking at lower stresses to more localized larger-scale cracking at higher stresses. Here we caution that we use the b-values qualitatively, as we

are not able to precisely locate individual AE events with the current experimental setup. Nevertheless, the general attitude of the rheological and seismogenic profiles was similar for every multiphase melt tested irrespective of their chemical components, crystal content, or temperature.

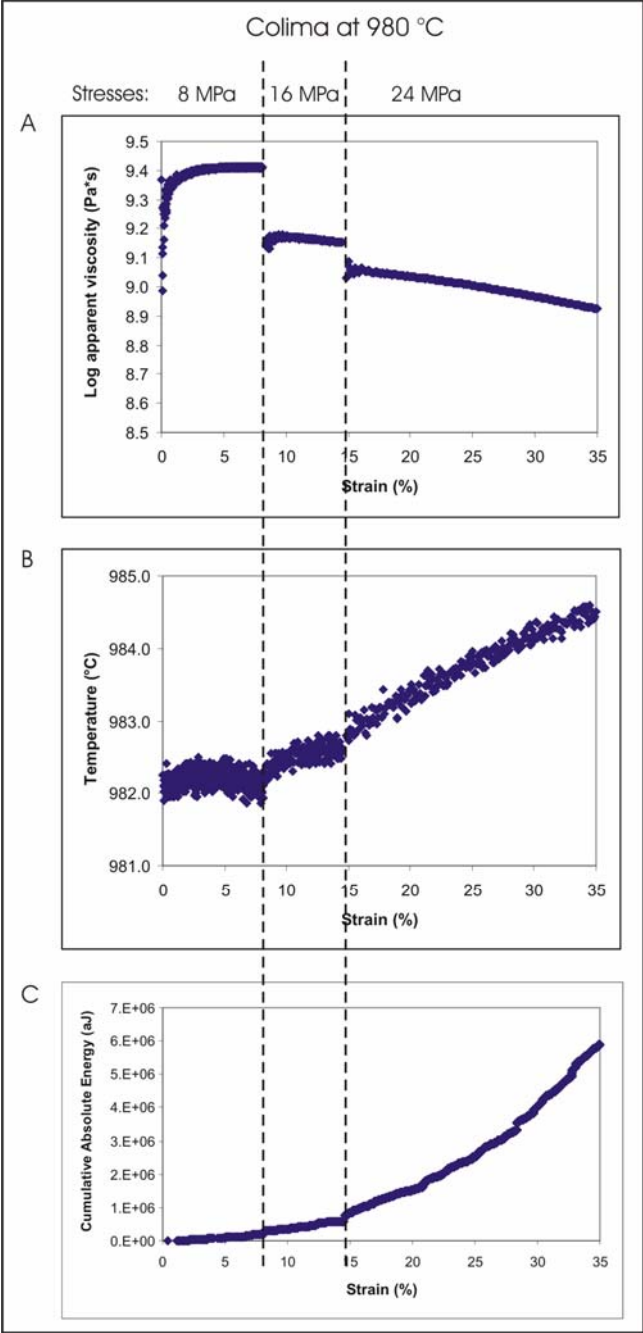


Figure 4-3. Experimental results for successive deformation of a Colima melt at 8, 16, and 24 MPa: (a) The apparent viscosity profile shows the instantaneous decrease associated with each stress increment. This is the origin of the non-Newtonian behaviour. (b) The internal melt temperature shows an increase associated with minor viscous heating at high stress. (c) The cumulative AE energy output is minor and constant at low to moderate stress and increase exponentially at high stress ($1 \text{ fJ} = 10^{-15} \text{ J}$).

Suspension rheology involves cracking throughout the spectrum. In general, the rates of AE output increases non-linearly with increasing strain rate and accelerates exponentially as failure is approached (Figure 4-4). The deformation is essentially aseismic at strain rates below 10^{-4} s^{-1} (a few minor AE are generated by internal rearrangement). The presence of crystals within a melt apparently significantly lowers the strain rate corresponding to the onset of the ductile-brittle transition in these multiphase magmas. Textural analysis of deformed samples indicates that cracking generally develops in plagioclase crystals; presumably because they are commonly twinned and zoned, and possesses important cleavage planes along $\{001\}$, $\{010\}$ and $\{110\}$. Textural analysis also reveals the alignment of crystals during deformation and the development of large-scale cracks at high strain rates (also reflected in the decrease of seismic b-value). Complementary quantitative analyses of fabrics developed in Colima and Bezymianny samples using the automated pattern analysis software AMOCADO (Gerik and Kruhl, submitted) revealed an increase in the overall anisotropy of the suspension by $\sim 29\%$ upon 33% strain (Figure 4-5). The anisotropy of the crystal phase however decreased by 19% . These observations suggest that during deformation, elongated crystals become broken into more equant fragments (lowering the crystal anisotropy) while the fragments from the original crystals align themselves perpendicularly to the applied stress to ease flow migration of the interstitial melt (increasing the overall anisotropy).

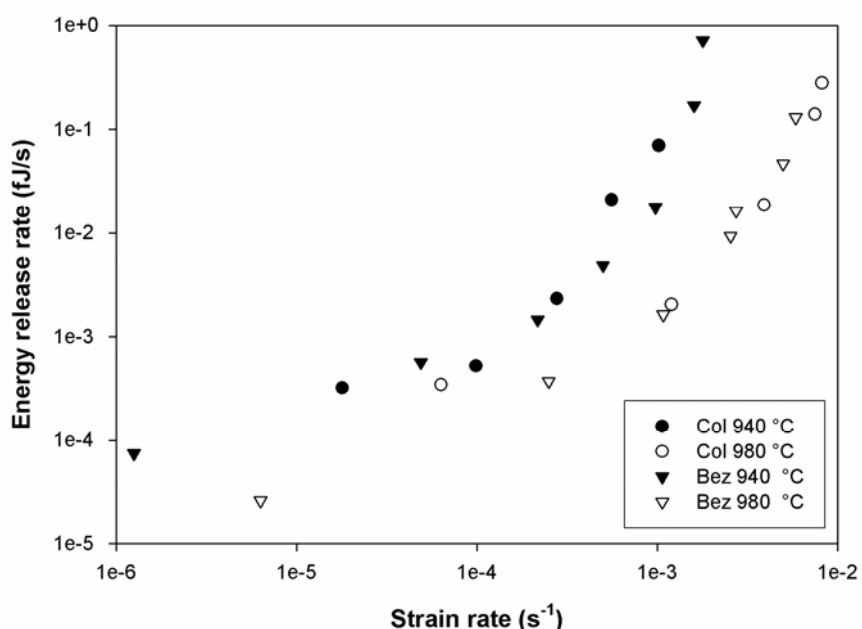


Figure 4-4. AE energy released rates for Colima and Bezymianny lavas at different strain rates. Although the crystallinities of Colima ($\sim 55\%$ crystals) and Bezymianny ($\sim 80\%$ crystals) melt samples were significantly different, the behaviour of both melts were very similar at a given temperature. It is rather the temperature which may serve to attenuate AE.

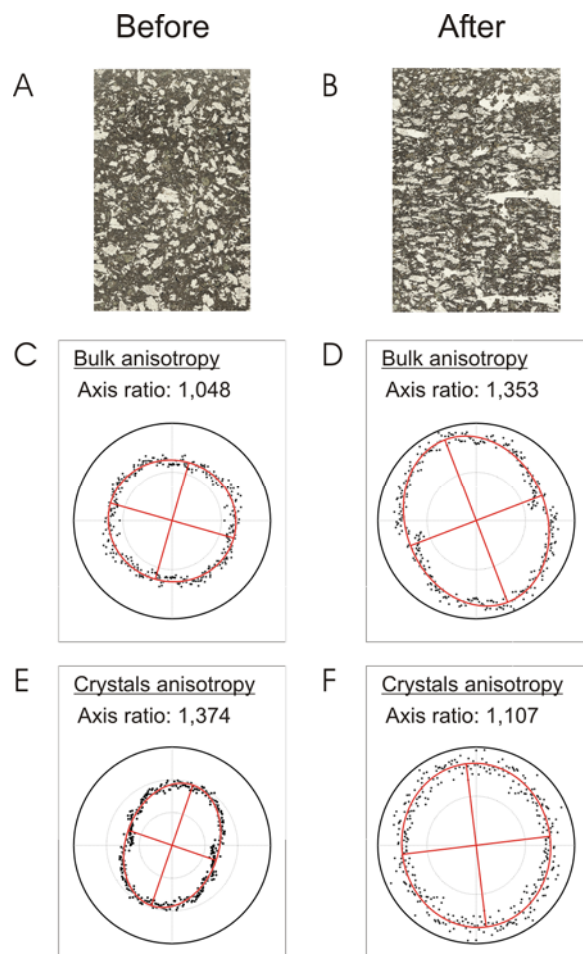


Figure 4-5. Anisotropic changes associated with deformation. These show the results of an experiment on Colima at 940 °C under 40 MPa. Photographs of thin sections (a) before the experiment, and (b) after the experiment (the applied stress was parallel with the long axis of the thin section). Both thin section were prepared along the same plane in the original rock sample. The post-experiment thin section shows a clear align of the crystals perpendicular to the applied stress. The anisotropy analysis of the whole the sample as a whole increased by 39% when comparing the axis ratios (c) before the experiment, and (d) after the experiment. In contrast, the anisotropy of the crystal phase alone decreased by 19%, when comparing the results (e) before and (f) after. These anisotropy graphs are direction vs slop plots for the intersection of segments with the analysed fabric. Each ring is equivalent to a count of (c) 500 units, (d) 1000 units, (e) 1250 units, and (f) 50 units (refer to the work of Gerik and Kruhl, submitted).

4.4. Application of the failure forecast method (FFM)

Given our observation that multiphase lavas behave brittlely at high strain rate, we have chosen to test whether crack growth and macroscopic failure of a multiphase melt at high strain rate is comparable to rock failure. The material failure forecast method (FFM) relies on the production rate of precursory phenomena (e.g., seismicity rate, AE rate, seismic

energy release, etc.), and correlating their accelerations to the likeliness of failure – in this case, of an eruption – via the equation

$$\frac{d^2\Omega}{dt^2} = A \left(\frac{d\Omega}{dt} \right)^\alpha \quad (10)$$

where $d^2\Omega/dt^2$ and $d\Omega/dt$ are the acceleration and rate of the phenomenon being monitored, and A and α are empirically determined parameters (Cornelius and Voight, 1995; De la Cruz-Reyna and Reyes-Davila, 2001; Kilburn, 2003; Tokarev, 1963; Voight, 1988). More explicitly α is expected to evolve from 1 to 2 before an eruption (Cornelius and Voight, 1995). Recent description of the fracturing time series that arise from random energy fluctuations within a finite volume subject to a constant remote stress proposed that the peaks in event rate (rather than all seismic events) predict best the path to failure and that $\alpha = 2$ when approaching failure (Kilburn, 2003). The equation can thus be simplified to:

$$\frac{1}{d\Omega/dt} = A(t_f - t) \quad (11)$$

where t_f is the expected time-to-failure. Since the acceleration increases before failure, the extrapolation of the inverse rate to zero should provide the time-to-failure. Although empirically derived from the field of rock mechanics, this approach appears to provide a good representation of precursory accelerations preceding natural eruptions (De la Cruz-Reyna and Reyes-Davila, 2001); especially, when the acceleration of energy released is used (Smith et al., 2007). However, the predictions yielded by the model remain uncertain until shortly before an eruption, and thus an improved treatment must unfortunately await better rheological and seismological constraints (Smith et al., 2007).

Our deformation experiments at very high strain rates on Colima lavas were characterized by clear exponential increases in the AE event rate and energy rate until complete failure soon thereafter. We can therefore retrieve a data distribution analogous to AE measured for rocks before failure by simply inverting the AE rate as shown in Figure 4-6. Extrapolations of the peak energy rate data points after four seconds yield indeed a very accurate prediction of the macroscopic failure of lava which occurred after twelve seconds. Although the test cannot be used to model more accurate α values at this point, it is strongly suggestive that the choice of an exponent equalling two and the use of peak energy values are appropriate for the forecasts of lavas dome eruption induced by shear strain. An earlier attempt to use the acceleration of seismic energy release to forecast two volcanic eruptions at Colima (July 1994 in hindsight and November 1998 in foresight) has shown that the method only became reasonably accurate shortly before the eruption (De la Cruz-Reyna and Reyes-Davila, 2001). That study further specifies that such forecasting models “require that the

medium be considered as a closed-continuum system”. Under such conditions, our work reveals the possibility of accurate early predictions. We attribute the difficulty of using the FFM in real-time during volcanic crisis to the use of seismic data which may not all originate from a common process. For instance, stick-slip motion along fault planes in the upper conduit (e.g., Mount St. Helens, Iverson et al., 2006) would alter the seismic signals derived from shear-induced fragmentation at greater depth. Such a signal distinction is an essential prerequisite to future forecasting attempts. The present findings indicate that runaway growth of the strain rate and seismic energy release rates prior to volcanic eruption is likely to be the result of lava crossing the ductile-brittle transition as a result of increasing strain rate.

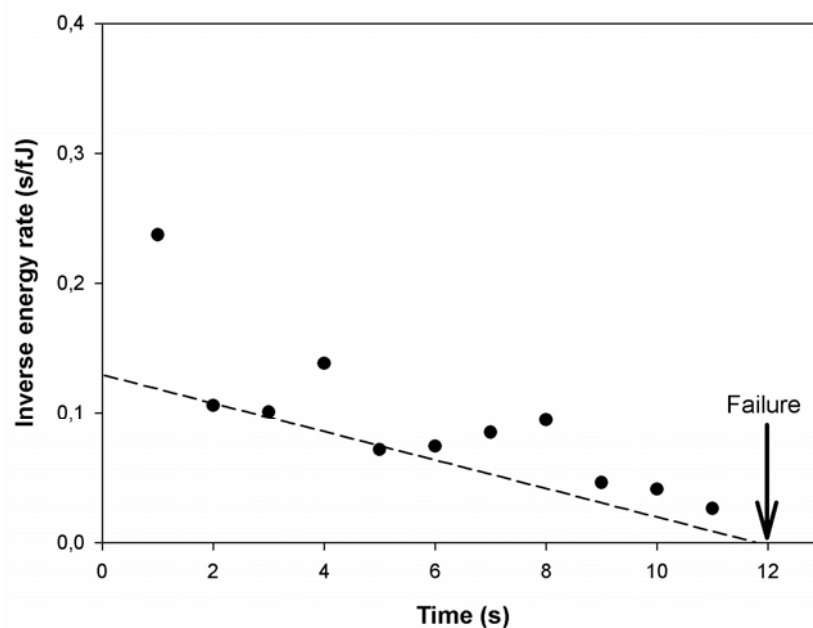


Figure 4-6. Application of the FFM on a Colima lava. Experiment at 940 °C deformed under 40 MPa (strain rate of $7 \times 10^{-3} \text{ s}^{-1}$). The FFM prediction was based on the extrapolation of peak energy rates (lower values on this inverse scale), following the work of Kilburn (2003). Extrapolation of peak energy rates after 4 seconds of deformation (dotted line) predicts well the time of complete failure (arrow).

This work may have high impact in the realm of eruption forecast modelling. This is the first time that a series of rheological and acoustic tests has been able to expose the strong seismogenic character of multiphase lavas across the ductile-brittle transitional field. Below 10^{-4} s^{-1} lavas are nearly aseismic. In contrast high-strain rate experiments clearly reveal an exponential increase in acoustic emission and a localization of the cracking until complete failure around 10^{-2} s^{-1} . Energy rate acceleration before failure at high strain rates directly supports the application of FFM to dome-building eruptions. We urge its immediate testing in volcanic unrest events worldwide.

“You’re under the soil
Yes, deep in the soil
So we’ll end with a whistle and end with a bang
and all of us fit in our places”
- Genesis

Chapter 5

CONCLUSIONS

5.1. Conclusions

A major leap was made in the rheologic and seismogenic description of highly-crystalline dome lavas across the ductile-brittle transition. This achievement resulted from the development, thorough calibration, and use of a high-temperature, high-load uniaxial press which allowed for high-accuracy viscosity measurements on large melt samples. The accuracy of +/-0.06 logarithmic units indeed permitted the distinction of three primordial rheological effects across the ductile-brittle transition: (1) a non-Newtonian fluidity characterized by an important component of shear thinning, and a singular dependence of apparent viscosity on strain rate; (2) an increasing heat production from viscosity energy dissipation with increasing strain rate; and (3) a continuous growth of microscopic cracks until the brittle regime prevails beyond a strain rate of 10^{-3} s^{-1} .

Cracking of the lavas was monitored by an acoustic sensor. Below a strain rate of about 10^{-4} s^{-1} lavas behave in a ductile manner and are essentially aseismic. At higher strain rates, crack growths and localization generate a commensurate exponential increase in micro-seismic activity, until complete brittle failure occurred at strain rates close to 10^{-2} s^{-1} . Application of the material failure forecasting method (FFM) to predict macroscopic failure of the melt using the acceleration of seismic energy release yielded very accurate predictions after 4 seconds of deformation (that is, 8 seconds before complete failure).

Ours findings on the rheology and seismology of multiphase dome lavas concur with the localization of strain along the volcanic conduit margin and therefore the development of plug-like flow. The rheological results coupled to the seismicity further support the association of seismic swarms with seismogenic shear zones during eruptions. This study therefore emphasise the need to carefully monitor the seismicity during volcanic unrest; in particularly, heed the acceleration of seismic energy release that can be use with failure forecast methods to successfully predict impending lava dome eruptions.

5.2. References

- Alidibirov, M. and Dingwell, D.B., 1996. Magma fragmentation by rapid decompression. *Nature*, 380(6570): 146-148.
- Alidibirov, M. et al., 1997. Physical properties of the 1980 Mount St. Helens cryptodome magma. *Bulletin of Volcanology*, 59(2): 103-111.
- Arzi, A.A., 1978. Fusion Kinetics, Water-Pressure, Water Diffusion and Electrical-Conductivity in Melting Rock, Interrelated. *Journal of Petrology*, 19(1): 153-169.
- Avery, J.G., 2003. The aftermath of a disaster - Recovery following the volcanic eruptions in Montserrat, West Indies. *West Indian Medical Journal*, 52(2): 131-135.
- Bagdassarov, N. and Dorfman, A., 1998. Granite rheology: magma flow and melt migration. *Journal of the Geological Society*, 155: 863-872.
- Bagdassarov, N.S. and Dingwell, D.B., 1992. A Rheological Investigation of Vesicular Rhyolite. *Journal of Volcanology and Geothermal Research*, 50(3): 307-322.
- Bouhifd, M.A., Richet, P., Besson, P., Roskosz, M. and Ingrin, J., 2004. Redox state, microstructure and viscosity of a partially crystallized basalt melt. *Earth and Planetary Science Letters*, 218(1-2): 31-44.
- Bruckner, R. and Deubener, J., 1997. Description and interpretation of the two phase flow behaviour of melts with suspended crystals. *Journal of Non-Crystalline Solids*, 209(3): 283-291.
- Burlini, L. et al., 2007. Seismicity preceding volcanic eruptions: New experimental insights. *Geology*, 35(2): 183-186.
- Byerlee, J. and Lockner, D., 1976. Measurement of Acoustic-Emission in Rock at High Confining Pressure and Differential Stress and Its Relation to Creep. *Transactions-American Geophysical Union*, 57(12): 1011-1011.
- Caricchi, L. et al., in press. Non-Newtonian rheology of crystal-bearing magmas and implications for magma ascent dynamics. *Earth and Planetary Science Letters*.
- Chmelik, F. et al., 2002. An evaluation of the creep characteristics of an AZ91 magnesium alloy composite using acoustic emission. *Materials Science and Engineering a-Structural Materials Properties Microstructure and Processing*, 338(1-2): 1-7.
- Chouet, B.A., 1996. Long-period volcano seismicity: Its source and use in eruption forecasting. *Nature*, 380(6572): 309-316.
- Cordonnier, B., Hess, K.U., Lavallee, Y. and Dingwell, D.B., Submitted. Rheology of Unzen dome lava.
- Cornelius, R.R. and Voight, B., 1995. Graphical and Pc-Software Analysis of Volcano Eruption Precursors According to the Materials Failure Forecast Method (Ffm). *Journal of Volcanology and Geothermal Research*, 64(3-4): 295-320.
- Costa, A., 2005. Viscosity of high crystal content melts: Dependence on solid fraction. *Geophysical Research Letters*, 32(22).
- Cox, S.J.D. and Meredith, P.G., 1993. Microcrack Formation and Material Softening in Rock Measured by Monitoring Acoustic Emissions. *International Journal of Rock Mechanics and Mining Sciences & Geomechanics Abstracts*, 30(1): 11-24.
- De la Cruz-Reyna, S. and Reyes-Davila, G.A., 2001. A model to describe precursory material-failure phenomena: applications to short-term forecasting at Colima volcano, Mexico. *Bulletin of Volcanology*, 63(5): 297-308.
- Deubener, J. and Bruckner, R., 1997. Influence of nucleation and crystallisation on the rheological properties of lithium disilicate melt. *Journal of Non-Crystalline Solids*, 209(1-2): 96-111.
- Dingwell, D.B., 1996. Volcanic dilemma: Flow or blow? *Science*, 273(5278): 1054-1055.

- Dingwell, D.B., 1998. Melt viscosity and diffusion under elevated pressures, *Ultrahigh-Pressure Mineralogy. Reviews in Mineralogy*, pp. 397-424.
- Dingwell, D.B., Hess, K.U. and Romano, C., 1998a. Extremely fluid behavior of hydrous peralkaline rhyolites. *Earth and Planetary Science Letters*, 158(1-2): 31-38.
- Dingwell, D.B., Hess, K.U. and Romano, C., 1998b. Viscosity data for hydrous peraluminous granitic melts: Comparison with a metaluminous model. *American Mineralogist*, 83(3-4): 236-239.
- Dobson, D.P., Meredith, P.G. and Boon, S.A., 2004. Detection and analysis of microseismicity in multi anvil experiments. *Physics of the Earth and Planetary Interiors*, 143-44: 337-346.
- Einstein, A., 1906. A new determination of the molecular dimensions. *Annalen Der Physik*, 19(2): 289-306.
- Einstein, A., 1911. A new determination of the molecular dimensions (vol 19, pg 289, 1906). *Annalen Der Physik*, 34(3): 591-592.
- Fontana, E.H., 1970. A Versatile Parallel-Plate Viscometer for Glass Viscosity Measurements to 1000 Degrees C. *American Ceramic Society Bulletin*, 49(6): 594-&.
- Gent, A.N., 1960. Theory of the Parallel Plate Viscometer. *British Journal of Applied Physics*, 11(2): 85-87.
- Gerik, A. and Kruhl, J.H., submitted. Towards automated pattern quantification: time-efficient assessment of anisotropy of 2D patterns with AMOCADO.
- Giordano, D. et al., 2006. An expanded non-Arrhenian model for silicate melt viscosity: A treatment for metaluminous, peraluminous and peralkaline liquids. *Chemical Geology*, 229(1-3): 42-56.
- Gonnermann, H.M. and Manga, M., 2003. Explosive volcanism may not be an inevitable consequence of magma fragmentation. *Nature*, 426(6965): 432-435.
- Goto, A., Oshima, H. and Nishida, Y., 1997. Empirical method of calculating the viscosity of peraluminous silicate melts at high temperatures. *Journal of Volcanology and Geothermal Research*, 76(3-4): 319-327.
- Harrington, R.M. and Brodsky, E.E., 2007. Volcanic hybrid earthquakes that are brittle-failure events. *Geophysical Research Letters*, 34(6).
- Hess, K.U., Cordonnier, B., Lavallée, Y. and Dingwell, D.B., 2007. High-load, high-temperature deformation apparatus for synthetic and natural silicate melts. *Review of Scientific Instruments*, 78.
- Hess, K.U., Cordonnier, B., Lavallée, Y. and Dingwell, D.B., submitted. Viscous heating in rhyolite: an in situ determination. *Earth and Planetary Science Letters*.
- Hess, K.U. and Dingwell, D.B., 1996. Viscosities of hydrous leucogranitic melts: A non-Arrhenian model. *American Mineralogist*, 81(9-10): 1297-1300.
- Holtz, F., Roux, J., Ohlhorst, S., Behrens, H. and Schulze, F., 1999. The effects of silica and water on the viscosity of hydrous quartzofeldspathic melts. *American Mineralogist*, 84(1-2): 27-36.
- Hui, H.J. and Zhang, Y.X., 2007. Toward a general viscosity equation for natural anhydrous and hydrous silicate melts. *Geochimica Et Cosmochimica Acta*, 71(2): 403-416.
- Iverson, R.M. et al., 2006. Dynamics of seismogenic volcanic extrusion at Mount St Helens in 2004-05. *Geology*, 444: 439-443.
- Kennedy, B. et al., 2005. Conduit implosion during Vulcanian eruptions. *Geology*, 33(7): 581-584.
- Kilburn, C.R.J., 2003. Multiscale fracturing as a key to forecasting volcanic eruptions. *Journal of Volcanology and Geothermal Research*, 125(3-4): 271-289.
- Knilljl, Franklin, J.A. and Malone, A.W., 1968. A Study of Acoustic Emission from Stressed Rock. *International Journal of Rock Mechanics and Mining Sciences*, 5(1): 87-&.

- Koerner, R.M., McCabe, W.M. and Lord, A.E., 1981. Overview of Acoustic-Emission Monitoring of Rock Structures. *Rock Mechanics*, 14(1): 27-35.
- Kueppers, U., Perugini, D. and Dingwell, D.B., 2006a. "Explosive energy" during volcanic eruptions from fractal analysis of pyroclasts. *Earth and Planetary Science Letters*, 248(3-4): 800-807.
- Kueppers, U., Scheu, B., Spieler, O. and Dingwell, D.B., 2006b. Fragmentation efficiency of explosive volcanic eruptions: A study of experimentally generated pyroclasts. *Journal of Volcanology and Geothermal Research*, 153(1-2): 125-135.
- Kumagai, H. and Chouet, B.A., 2000. Acoustic properties of a crack containing magmatic or hydrothermal fluids. *Journal of Geophysical Research-Solid Earth*, 105(B11): 25493-25512.
- Lacroix, A., 1902. About the ash of the eruption of the Pelee Mountain in 1851 and 1902. *Comptes Rendus Hebdomadaires Des Seances De L Academie Des Sciences*, 134: 1327-1329.
- Lavallée, Y., Hess, K.U., Cordonnier, B. and Dingwell, D.B., 2007. A non-Newtonian rheological law for highly-crystalline dome lavas. *Geology*, 35: 843-846.
- Lejeune, A.M. and Richet, P., 1995. Rheology of Crystal-Bearing Silicate Melts - an Experimental-Study at High Viscosities. *Journal of Geophysical Research-Solid Earth*, 100(B3): 4215-4229.
- Lockner, D. and Byerlee, J., 1977. Acoustic-Emission and Creep in Rock at High Confining Pressure and Differential Stress. *Bulletin of the Seismological Society of America*, 67(2): 247-258.
- Main, I.G., Sammonds, P.R. and Meredith, P.G., 1993. Application of a Modified Griffith Criterion to the Evolution of Fractal Damage During Compressional Rock Failure. *Geophysical Journal International*, 115(2): 367-380.
- Manns, P. and Bruckner, R., 1988. Non-Newtonian Flow Behavior of a Soda Lime Silicate Glass at High Deformation Rates. *Glastechnische Berichte-Glass Science and Technology*, 61(2): 46-56.
- McBirney, A.R. and Murase, T., 1984. Rheological Properties of Magmas. *Annual Review of Earth and Planetary Sciences*, 12: 337-357.
- McNutt, S.R., 2005. Volcanic seismology. *Annual Review of Earth and Planetary Sciences*, 33: 461-491.
- Melnik, O. and Sparks, R.S.J., 1999. Nonlinear dynamics of lava dome extrusion. *Nature*, 402(6757): 37-41.
- Melosh, H.J., 1996. Dynamical weakening of faults by acoustic fluidization. *Nature*, 379(6566): 601-606.
- Meredith, P.G., Knight, K.S., Boon, S.A. and Wood, I.G., 2001. The microscopic origin of thermal cracking in rocks: An investigation by simultaneous time-of-flight neutron diffraction and acoustic emission monitoring. *Geophysical Research Letters*, 28(10): 2105-2108.
- Mueller, S., 2007. Permeability and porosity as constraints on the explosive eruption of magma: Laboratory experiments and field investigations. Ph.D. Thesis, Ludwig-Maximilians University, Munich, 149 pp.
- Mueller, S., Melnik, O., Spieler, O., Scheu, B. and Dingwell, D.B., 2005. Permeability and degassing of dome lavas undergoing rapid decompression: An experimental determination. *Bulletin of Volcanology*, 67(6): 526-538.
- Mueller, S., Spieler, O., Scheu, B. and Dingwell, D.B., 2004. A new method for unsteady-state permeability measurements of volcanic rocks at high temperature. *Lithos*, 73(1-2): S77-S77.
- Murase, T., McBirney, A.R. and Melson, W.G., 1985. Viscosity of the Dome of Mount St-Helens. *Journal of Volcanology and Geothermal Research*, 24(1-2): 193-204.

- Neuberg, J., 2000. Characteristics and causes of shallow seismicity in andesite volcanoes. *Philosophical Transactions of the Royal Society of London Series a-Mathematical Physical and Engineering Sciences*, 358(1770): 1533-1546.
- Neuberg, J., Luckett, R., Baptie, B. and Olsen, K., 2000. Models of tremor and low-frequency earthquake swarms on Montserrat. *Journal of Volcanology and Geothermal Research*, 101(1-2): 83-104.
- Neuville, D.R. and Richet, P., 1991. Viscosity and Mixing in Molten (Ca, Mg) Pyroxenes and Garnets. *Geochimica Et Cosmochimica Acta*, 55(4): 1011-1019.
- Ohnaka, M., 1983. Acoustic-Emission During Creep of Brittle Rock. *International Journal of Rock Mechanics and Mining Sciences*, 20(3): 121-134.
- Ojala, I.O., Main, I.G. and Ngwenya, B.T., 2004. Strain rate and temperature dependence of Omori law scaling constants of AE data: Implications for earthquake foreshock-aftershock sequences. *Geophysical Research Letters*, 31(24).
- Ostwald, W., 1925. Concerning the function rate of the viscosity of dispersion systems. IV. *Kolloid-Zeitschrift*, 36(4): 248-250.
- Papale, P., 1999a. Numerical simulations of magma ascent along volcanic conduits. *Physics and Chemistry of the Earth Part a-Solid Earth and Geodesy*, 24(11-12): 957-961.
- Papale, P., 1999b. Strain-induced magma fragmentation in explosive eruptions. *Nature*, 397(6718): 425-428.
- Petford, N., 2003. Rheology of granitic magmas during ascent and emplacement. *Annual Review of Earth and Planetary Sciences*, 31: 399-427.
- Pinkerton, H. and Norton, G., 1995. Rheological Properties of Basaltic Lavas at Sub-Liquidus Temperatures - Laboratory and Field-Measurements on Lavas from Mount Etna. *Journal of Volcanology and Geothermal Research*, 68(4): 307-323.
- Pinkerton, H. and Stevenson, R.J., 1992. Methods of Determining the Rheological Properties of Magmas at Sub-Liquidus Temperatures. *Journal of Volcanology and Geothermal Research*, 53(1-4): 47-66.
- Prikryl, R., Lokajicek, T., Li, C. and Rudajev, V., 2003. Acoustic emission characteristics and failure of uniaxially stressed granitic rocks: The effect of rock fabric. *Rock Mechanics and Rock Engineering*, 36(4): 255-270.
- Quane, S.L., Russell, J.K. and Kennedy, L.A., 2004. A low-load, high-temperature deformation apparatus for volcanological studies. *American Mineralogist*, 89(5-6): 873-877.
- Ramos, J.I., 1999. Two-dimensional simulations of magma ascent in volcanic conduits. *International Journal for Numerical Methods in Fluids*, 29(7): 765-789.
- Richard, D., Scheu, B., Mueller, S., Spieler, O. and Dingwell, D.B., 2006. Factors Controlling the Fragmentation Behavior of Magma, American Geophysical Union. *Eos Trans.*
- Roscoe, R., 1952. The Viscosity of Suspensions of Rigid Spheres. *British Journal of Applied Physics*, 3(AUG): 267-269.
- Rosenberg, C.L., 2004. Shear zones and magma ascent: A model based on a review of the Tertiary magmatism in the Alps. *Tectonics*, 23(3).
- Rowe, C.A., Thurber, C.H. and White, R.A., 2004. Dome growth behavior at Soufriere Hills Volcano, Montserrat, revealed by relocation of volcanic event swarms, 1995-1996. *Journal of Volcanology and Geothermal Research*, 134(3): 199-221.
- Ryan, M.P. and Blevins, J.Y.K., 1987. Viscosity of synthetic and natural silicate melts and glasses. *U.S. Geological Survey Bulletin*, 1764: 563.
- Ryerson, F.J., Weed, H.C. and Piwinski, A.J., 1988. Rheology of Subliquidus Magmas .1. Picritic Compositions. *Journal of Geophysical Research-Solid Earth and Planets*, 93(B4): 3421-3436.

- Saar, M.O., Manga, M., Cashman, K.V. and Fremouw, S., 2001. Numerical models of the onset of yield strength in crystal-melt suspensions. *Earth and Planetary Science Letters*, 187(3-4): 367-379.
- Scaillet, B., Holtz, F., Pichavant, M. and Schmidt, M., 1996. Viscosity of Himalayan leucogranites: Implications for mechanisms of granitic magma ascent. *Journal of Geophysical Research-Solid Earth*, 101(B12): 27691-27699.
- Scheu, B., Kueppers, U., Mueller, S., Spieler, O. and Dingwell, D.B., 2007. Experimental volcanology on eruptive products of Unzen.
- Schulze, F., Behrens, H., Holtz, F., Roux, J. and Johannes, W., 1996. The influence of H₂O on the viscosity of a haplogranitic melt. *American Mineralogist*, 81(9-10): 1155-1165.
- Schulze, F., Behrens, H. and Hurkuck, W., 1999. Determination of the influence of pressure and dissolved water on the viscosity of highly viscous melts: Application of a new parallel-plate viscometer. *American Mineralogist*, 84(10): 1512-1520.
- Smith, R., Kilburn, C.R.J. and Sammonds, P.R., 2007. Rock fracture as a precursor to lava dome eruptions at Mount St Helens from June 1980 to October 1986. *Bulletin of Volcanology*, 69(6): 681-693.
- Sparks, R.S.J., 2003. Forecasting volcanic eruptions. *Earth and Planetary Science Letters*, 210(1-2): 1-15.
- Spera, F.J., 2000. Physical properties of magmas. In: H. Sigurdsson, B. Houghton, S.R. McNutt, H. Rymer and J. Styx (Editors), *Encyclopedia of Volcanoes*. Academic, San Diego, pp. 171-190.
- Spieler, O. et al., 2004. The fragmentation threshold of pyroclastic rocks. *Earth and Planetary Science Letters*, 226(1-2): 139-148.
- Stein, D.J. and Spera, F.J., 2002. Shear viscosity of rhyolite-vapor emulsions at magmatic temperatures by concentric cylinder rheometry. *Journal of Volcanology and Geothermal Research*, 113(1-2): 243-258.
- Stevenson, R.J., Bagdassarov, N.S., Dingwell, D.B. and Romano, C., 1998. The influence of trace amounts of water on the viscosity of rhyolites. *Bulletin of Volcanology*, 60(2): 89-97.
- Stevenson, R.J., Dingwell, D.B., Webb, S.L. and Bagdassarov, N.S., 1995. The Equivalence of Enthalpy and Shear-Stress Relaxation in Rhyolitic Obsidians and Quantification of the Liquid-Glass Transition in Volcanic Processes. *Journal of Volcanology and Geothermal Research*, 68(4): 297-306.
- Stevenson, R.J., Dingwell, D.B., Webb, S.L. and Sharp, T.G., 1996. Viscosity of microlite-bearing rhyolitic obsidians: An experimental study. *Bulletin of Volcanology*, 58(4): 298-309.
- Tanguy, J.C., 1994. The 1902-1905 Eruptions of Montagne-Pelee, Martinique - Anatomy and Retrospection. *Journal of Volcanology and Geothermal Research*, 60(2): 87-107.
- Tokarev, P., 1963. On a possibility of forecasting of Bezymianny volcano eruptions according to seismic data. *Bulletin of Volcanology*, 26: 379-386.
- Tuffen, H. and Dingwell, D.B., 2005. Fault textures in volcanic conduits: evidence for seismic trigger mechanisms during silicic eruptions. *Bulletin of Volcanology*, 67(4): 370-387.
- Tuffen, H., Dingwell, D.B. and Pinkerton, H., 2003. Repeated fracture and healing of silicic magma generate flow banding and earthquakes? *Geology*, 31(12): 1089-1092.
- van der Molen, I. and Paterson, M.S., 1979. Experimental Deformation of Partially-Melted Granite. *Contributions to Mineralogy and Petrology*, 70(3): 299-318.
- Vignerresse, J.L. and Tikoff, B., 1999. Strain partitioning during partial melting and crystallizing felsic magmas. *Tectonophysics*, 312(2-4): 117-132.
- Voight, B., 1988. A Method for Prediction of Volcanic-Eruptions. *Nature*, 332(6160): 125-130.

- Voight, B., 1989. A Relation to Describe Rate-Dependent Material Failure. *Science*, 243(4888): 200-203.
- Webb, S.L. and Dingwell, D.B., 1990. The Onset of Non-Newtonian Rheology of Silicate Melts - a Fiber Elongation Study. *Physics and Chemistry of Minerals*, 17(2): 125-132.
- White, R.A., Miller, A.D., Lynch, L. and Power, J., 1998. Observations of hybrid seismic events at Soufriere Hills Volcano, Montserrat: July 1995 to September 1996. *Geophysical Research Letters*, 25(19): 3657-3660.
- Wickham, S.M., 1987. The Segregation and Emplacement of Granitic Magmas. *Journal of the Geological Society*, 144: 281-297.

CURRICULUM VITAE

Personal Information

Yan Lavallée, Born on Thursday, 12 October 1978 in St-Jérôme, Québec, Canada

Education

- 2004 to 2008 **Doctor rerum naturalium in Volcanology through the Elite Network of Bavaria**
Ludwig-Maximilians University, Munich, Germany
- 2002 to 2003 **Master of Science in Space Studies**
University of North Dakota, Grand Forks, USA
- 1998 to 2001 **Bachelor of Science (Honours) in Earth and Planetary Sciences**
McGill University, Montréal, Canada
- 1996 to 1998 **Diplôme d'Études Collégiales in Sciences**
Collège de St-Jérôme, St-Jérôme, Canada
-

Work experiences

- 2004 to 2008 **Ludwig-Maximilians University, Munich, Germany**
 - Development of a high-load, high-temperature deformation apparatus for volcanological study. This promotes a unique approach to study dome lavas rheology and seismogenicity.
- Summer 2004 **McGill University, Montreal, Canada**
 - Assessing whether magma recharges facilitate the generation of voluminous eruptions at Yellowstone. This study coupled field work with preliminary experiments of magma recharge using corn sirup as magma analogue.
- 2002 to 2004 **University of North Dakota, Grand Forks, USA**
 - Investigating the absence of equivalent caldera collapse during the large 1600 explosive eruption of Huaynaputina, Peru. This study involved extensive field surveys, and analysis of remote sensing images and earthquake distribution.
 - Content editor of the VolcanoWorld website.
 - Reducing asteroids' spectral data acquired at Hawai'i observatory.
- Jul to Dec 2001 **McGill University, Montreal, Canada**
 - Investigating magmatic processes, through petrographical and structural analyses, of the caldera subsidence at Ossipee Ring Complex, USA.
 - Development of a virtual dictionary of petrology and volcanology.
- Summer 2000 **Geological Survey of Canada, Quebec, Canada**
 - Researcher, mapping and sampling the Grenville province, Quebec; a supracrustal area, with high-grade metamorphism.
- 1999 to 2000 **McGill University, Montreal, Canada**
 - Assistant in the development and analysis of analogue caldera experiments.
- Summer 1999 **University of Montreal, Montreal, Canada**
 - Mapping volcanoclastic deposits and structures of Cotopaxi volcano, Ecuador.
- Summer 1998 **ALSTOM Canada, Montreal, Canada**
 - Responsible of environmental issues; e.g., soil decontamination
 - Performing chemical tests to optimize industrial operations